Hydrodynamics and Scale-up of Coal Liquefaction Reactor

小野崎, 正樹
九州大学工学応化機能材料物性工学

https://doi.org/10.11501/3172442

出版情報：九州大学, 2000, 博士（工学）, 課程博士
バージョン：
権利関係：

Hydrodynamics and Scale-up of Coal Liquefaction Reactor

Onozaki, Masaki.

Hydrodynamics and Scale-up of Coal Liquefaction Reactor

石炭液化反応塔の流動およびスケールアップ

By

Masaki Onozaki

小 野 﨑 正 樹

A dissertation
submitted in partial fulfillment
of the requirements for the degree of
Doctor of Engineering

Kyushu University
6-10-1 Hakozaki, Higashi-ku
Fukuoka 812-8581, Japan

2000

Table of Contents

List of Tables

List of Figures

1. Introduction

1.1 Objectives

According to the BP Amoco[1)], the world total primary energy consumption in 1998 was 8,477 million tons oil equivalent, 40% of which was crude oil and 20 % was coal. The IEA/OECD[2)] suggests that the total world energy demand will increase by 65 % between 1995 and 2020 as developing countries raise their standard of living. After the production of crude oil is maximized between 2010 and 2020, according to IEA[3,4)], coal will gradually take over crude oil's market share in the future.

The world has experienced two oil crises since 1973. The rising oil prices and the decreasing oil production rate accelerated the development of coal conversion technologies. Japan initiated the research and development of coal liquefaction as a national project under the "Sunshine Program" of the Ministry of International Trade and Industry (MITI). The basis of the NEDOL process as a liquefaction process has been established through bench scale plants, as well as basic studies supported by the New Energy and Industrial Technology Development Organization (NEDO). A coal liquefaction pilot plant with a capacity of 150 tons-coal/day was constructed in Kashima, Ibaraki, to obtain engineering data for the design of demonstration and commercial plants, as well as to confirm the performance of the process. Construction began in 1991 and finished in 1996. It was then operated without serious troubles for two years[5-7)].

The Kashima pilot plant was equipped with three bubble column reactors connected in series, each of which was 1 m in diameter and 11.8 m in length. The hydrodynamic behavior of the coal liquefaction reactors in the Exxon Donor Solvent Process (EDS), Solvent Refined Coal-II Process (SRC-II), and Nippon Brown Coal Liquefaction Process (NBCL) pilot plants were studied with tracers[8-11)], and the results showed that gas holdups in the reactors were significantly larger and liquid-phase axial dispersion coefficients were smaller than those obtained in bubble columns for air-water systems operated at an ambient pressure and temperature.

The objectives of this dissertation are to analyze the performance of the Kashima pilot plant using Tanitoharum coal, and to develop a design procedure for a large scale plant based on the NEDOL process.

The dissertation is divided into nine chapters. In the first chapter, the pilot plant project of the NEDOL process is introduced and the coal liquefaction reactors of the pilot plant are described. In the second chapter, characterization of the hydrodynamics of the liquefaction reactors are discussed based on the experimental data of the pilot plant. In the third chapter, the steady-state thermal behavior of coal liquefaction reactors is discussed via modeling the reactor. In the fourth chapter, gas-liquid dispersion behavior in the reactor is clarified using computational fluid dynamics. In the fifth chapter, the accumulation of solid particles in the first reactor is reported and the nature of the solids is discussed based on the analytical data. In the sixth chapter, the phenomenon of the solid accumulation is studied by computer simulation. In the seventh chapter, a process simulation of the coal liquefaction process is developed. In the eighth chapter, a scale-up procedure is proposed based on the hydrodynamics and liquefaction performance. In the ninth and final chapter, the above results are summarized.

1.2 Pilot Plant Work of the NEDOL Process

A coal liquefaction pilot plant having a capacity of 150 tons-coal/day was successfully operated from 1996 to 1998 in Kashima, Japan. Figure 1-1 shows a simplified process flow of the NEDOL process. Figure 1-2 shows more detailed information on the Kashima Pilot Plant. As shown in these figures, the pilot plant consists of four sections, first, the coal slurry preparation section including pulverizing, drying and mixing of the coal, second, the liquefaction section including a preheating unit and a high pressure separator, third, the distillation section with atmospheric and vacuum towers, and fourth, the solvent hydrogenation section which is comprised of a solvent hydrogenation reactor with six Ni/Mo catalyst beds. The goal of this project was to obtain scale-up engineering data, and to demonstrate the reliability of the NEDOL Process developed by the New Energy and Industrial Technology Development Organization (NEDO), Japan. The NEDOL Process involves the use of a fine pyrite catalyst12) and the hydrogenation of recycled oil at a connected plant13,14), and realizes high oil yields (58 wt% of the dry and ash-free coal) under mild reaction conditions (pressure = 16.8-18.8 MPa; temperature = 723-735 K). Although five runs have been performed for three different coals at the Kashima plant, this study is concerned with the data obtained using Tani-toharum subbituminous coal from Indonesia.

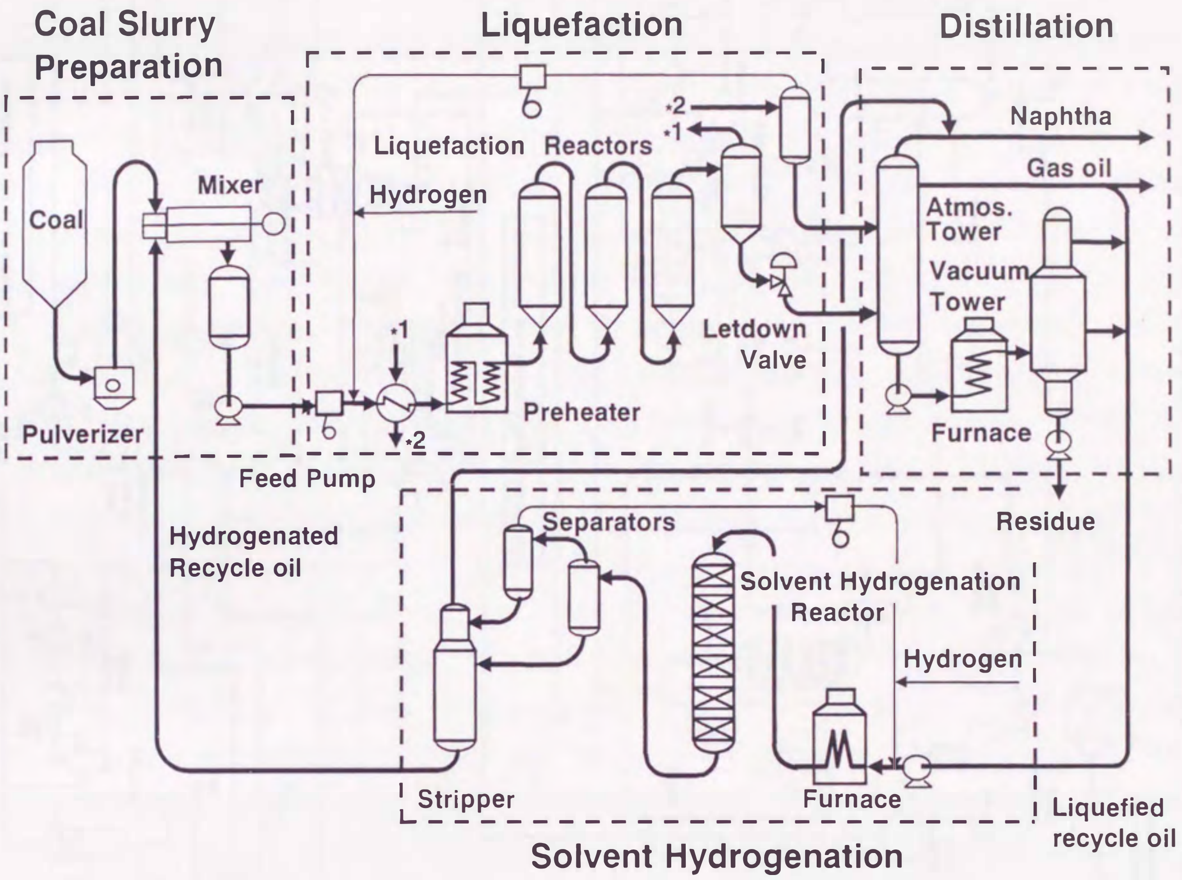

Figure 1-1. Process flow of NEDOL process.

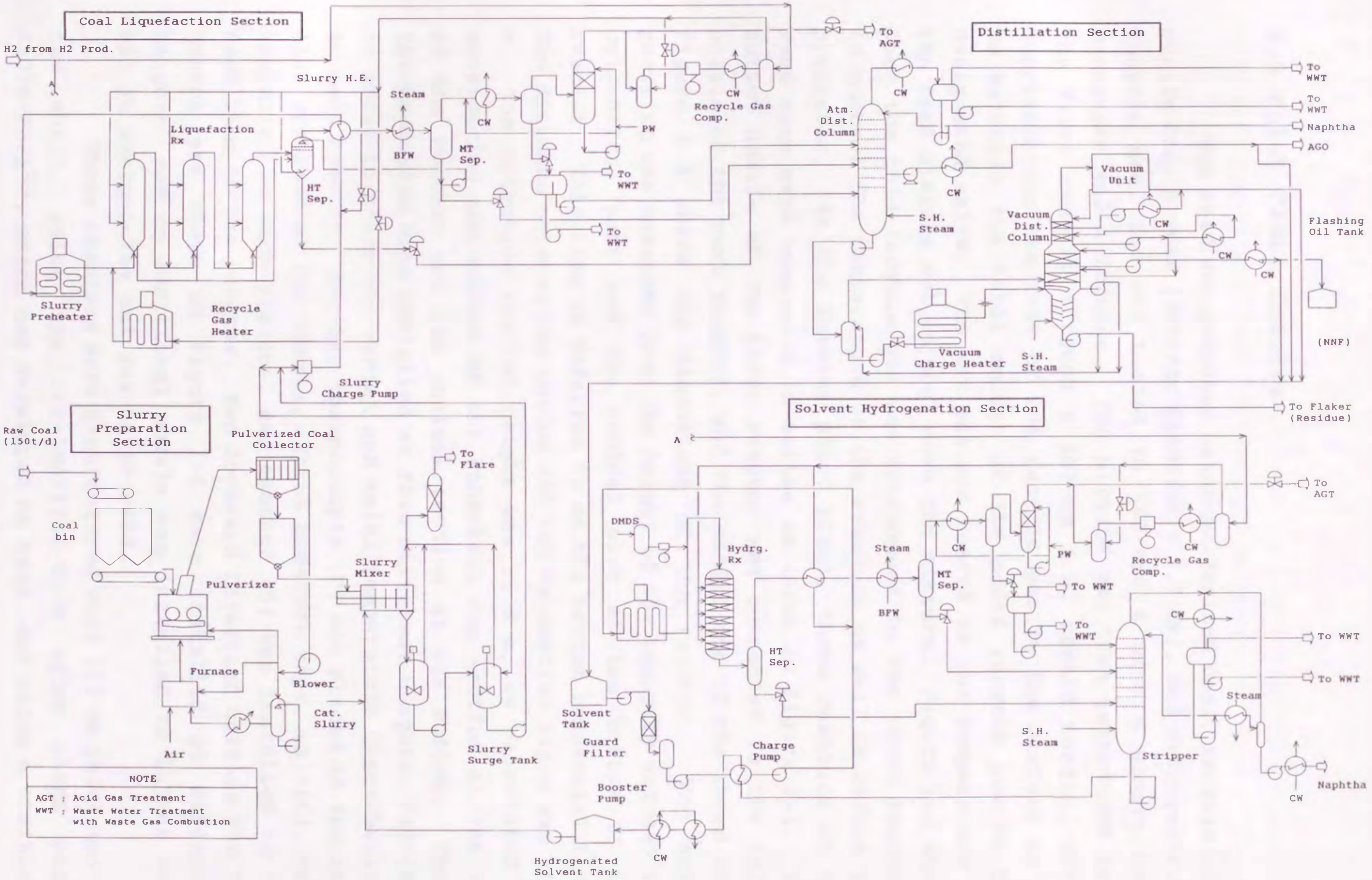

Figure 1-2. Process flow of 150 t/d Kashima Pilot Plant

1.3 Pilot Plant Reactor

The feed was prepared using pulverized coal, recycle oil, pyrite fine powder (average diameter = 0.7 μm), and hydrogen-rich recycle gas, and was heated to 660-690 K with a slurry heat exchanger and a furnace. The mixture was then introduced into the first reactor through a 107-mm i.d. upward nozzle, after supplementing the rest of hot recycle gas to the mixture so as to maintain the total amount of the added recycle gas to the designated value. The hot gas was heated to the temperature of the feed mixture not to cool down the mixture. Figure 1-3 shows that the cold recycle gas was introduced to the three reactors to control the temperature of the reactors as well as before the preheater. At the Kashima pilot plant, three reactors of the same size were connected in series as shown in Figure 1-1. The outlet nozzle of the first reactor was connected to the inlet nozzle of the next reactor, and the second one to the third one. Figure 1-4 shows the dimensions of the reactor. The axial position was measured from the height of the boundary between the cylindrical part and the conical part at the bottom of the reactor. This line is referred to as the bottom tangential line. The distance between the bottom and top tangential lines was 11.0 m. The effective reactor height was 11.8 m, as calculated by considering the volume of the spherical cap section at the top of the reactor and the conical section at the bottom. Three thermocouples were installed at five different heights, (A)-(E), in order to check the radial and axial temperature distributions in each reactor. Another thermocouple (F) was placed in the feed line upstream of the nozzle. Three pressure taps, (A)-(C), were installed in each reactor, and another (D) was installed in the feed line to the reactor. Two downward injection nozzles for the quench gas shown in Figure 1-4 were installed at different heights, and an additional nozzle was installed to inject cold oil in emergencies but was never used.

These reactors were manufactured with 113 mm thickness of the shell, using the 3Cr-1Mo-1/4V-Ti-B alloy (ASME code; SA336-F3V)$^{15)}$, which was developed by NEDO, and using a stainless steel 347 overlay. The reactor walls were thermally insulated with a 150 mm thick layer of calcium silicate.

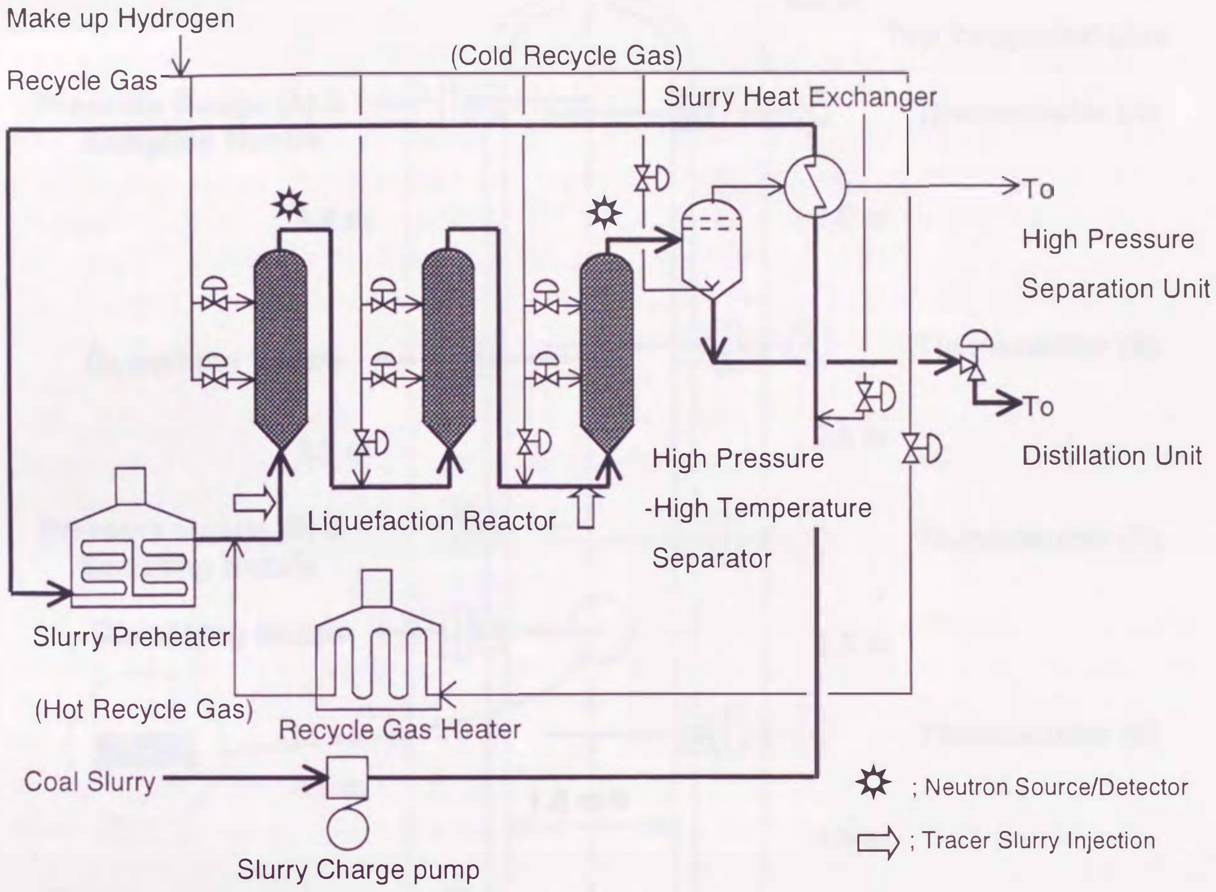

Figure 1-3. Process flow in liquefaction reactors.

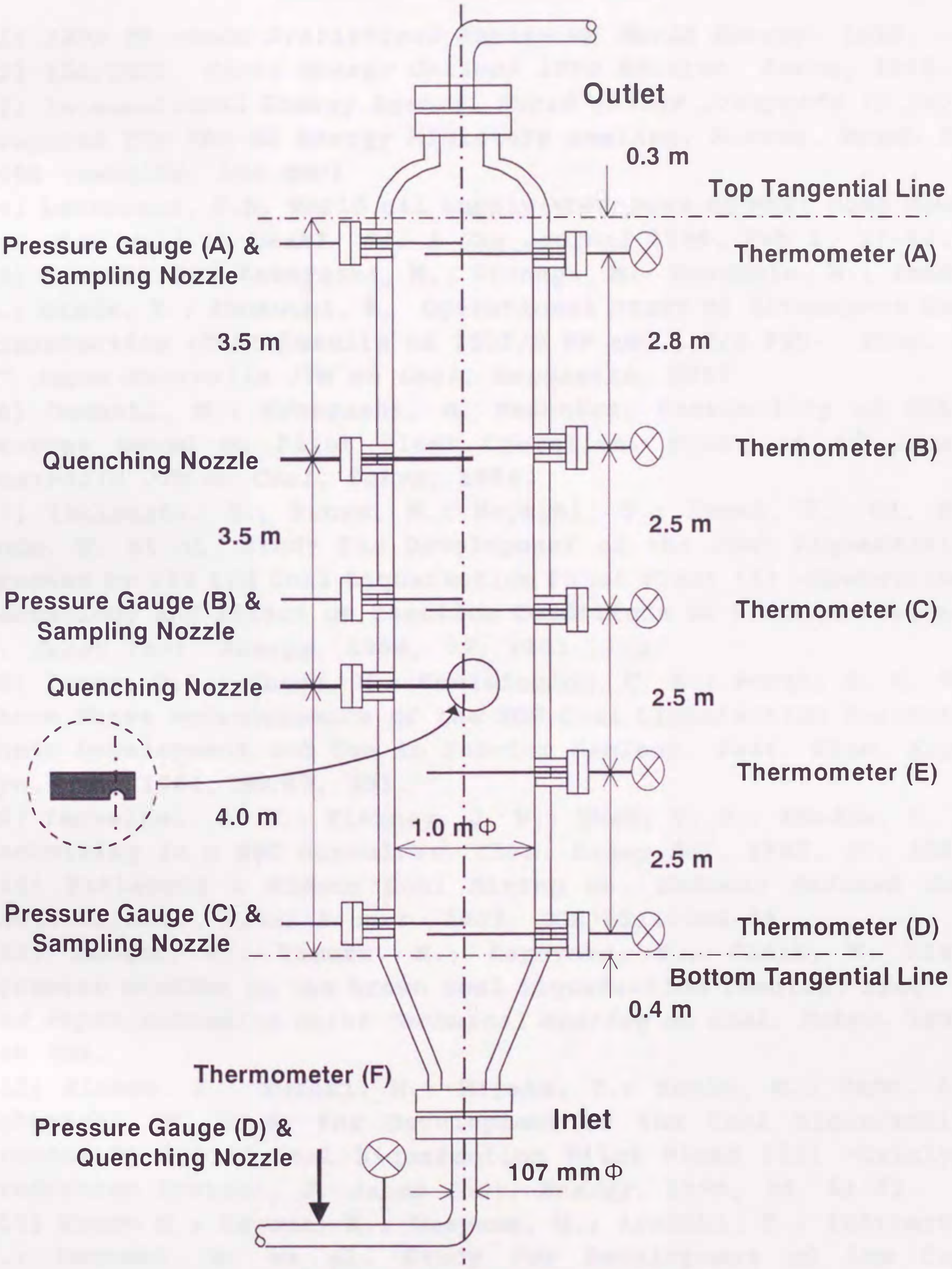

Figure 1-4. Dimensions of the liquefaction reactors.

References

(1) *1999 BP Amoco Statistical Review of World Energy*, 1999.

(2) IEA/OECD *World Energy Outlook 1998 Edition, Paris*, 1998.

(3) International Energy Agency *World energy prospects to 2020*. prepared for the G8 Energy Ministers meeting, Moscow, Mrach 31, 1998 (website: iea.gov)

(4) Laherrere, J.H. World oil supply-what goes up must come down, but when will it peak? *Oil & Gas Journal* **1999**, Feb 1, 57-64.

(5) Onozaki, M.; Kobayashi, M.; Itonaga, M.; Kawabata, M.; Imada, K.; Okada, Y.; Inokuchi, K. Operational Study of Bituminous Coal Liquefaction -Test Results of 150T/D PP and 1 T/D PSU-. *Proc. of 7th Japan-Australia JTM on Coal, Newcastle*, **1997**

(6) Onozaki, M.; Kobayashi, M. Technical Feasibility of NEDOL Process based on Pilot Plant Operation. *Proc. of 8th Japan-Australia JTM on Coal, Tokyo*, **1998**.

(7) Ishibashi, H.; Kouzu, M.; Hayashi, T.; Kamei, T.; Oi, S.; Endo, M. et al. Study for Development of the Coal Liquefaction Process by 150 t/d Coal Liquefaction Pilot Plant (I) -Operational Technology and Effect of Reaction Conditions on Product Yields-. *J. Japan Inst. Energy*, **1998**, *77*, 1201-1213.

(8) Tarmy, B.L.; Chang, M.; Coulaloglou, C. A.; Ponzi, P. R. The Three Phase Hydrodynamics of the EDS Coal Liquefaction Reactors: Their Development and Use in Reactor Scaleup. *Inst. Chem. Eng., Sym. Ser.* **1984**, No.87, 303.

(9) Panvelker, S. V.; Tierney, J. W.; Shah, Y. T.; Rhodes, D. F. Backmixing in a SRC dissolver. *Chem. Engng Sci.* **1982**, *37*, 1582.

(10) Pittsburg & Midway Coal Mining Co. *Solvent Refined Coal (SRC) Process, Final Report.* **1982**, DOE/ET/10104-46.

(11) Tanaka, Y.; Tamura, M.; Kageyama, H.; Clark, K. Fluid dynamics studies in the brown coal liquefaction reactor. *Proc. of 2nd Japan/Australia Joint Technical Meeting on Coal, Tokyo*, **1992**, 198-204.

(12) Hirano, K.; Suzuki, N.; Miyake, Y.; Kouzu, M.; Ueda, S.; Kobayashi, M. Study for Development of the Coal Liquefaction Process by 150t/d Coal Liquefaction Pilot Plant (II) -Catalyst Production System-. *J. Japan Inst. Energy*, **1999**, *78*, 42-52.

(13) Kouzu M.; Koyama, K.; Oneyama, M.; Aramaki, T.; Ishibashi, H.; Onozaki, M. et al. Study for Development of the Coal Liquefaction Process by 150t/d Coal Liquefaction Pilot Plant (IV). *J. Japan Inst. Energy*, **1999**, *78*, 120-128.

(14) Kouzu, M.; Koyama, K.; Oneyama, M.; Aramaki, T.; Hayashi, T.; Kobayashi, M.; Itoh, H.; Hattori, H. Catalytic hydrogenation of recycle solvent in a 150t/d pilot plant of the NEDOL coa

liquefaction process. *Fuel,* **2000**, *79*, 365-371.

(15) Tahara, T.; Ishiguro, T.; Iga, H; Hasegawa, T. Recent Technical Trends for Hydrotreating Reactors. *Nihon Seikoujo Giho*, **1995**, *51*, (4), 1-11.

2. Characterization of Hydrodynamics of Coal Liquefaction Reactors

2.1 Introduction

Bubble columns with gas-liquid-solid systems as well as gas-liquid systems are widely used in chemical and petrochemical industries. Comprehensive reviews on fundamental studies of transport phenomena as well as hydrodynamics in bubble columns or three-phase fluidization systems are available[1,2]. After Tarmy et al.[3] reported that the behaviors of hydrodynamics in coal liquefaction reactors, suspended bubble columns, under high pressure were different from those at the ambient conditions, the several areas of high-pressure bubble columns including the bubble dynamics, the macroscopic hydrodynamics properties, and three-phase fluidized beds have been focused. A specific review regarding high-pressure systems was made by Fan et al.[4].

In this chapter, the common data used for analyses of the pilot plant reactors and discussion for a large-scale reactor are described prior to the successive chapters. First, operating conditions of the liquefaction reactors are shown. Physical properties of the gas and slurry phases are discussed based on the experimental values and prediction methods. Experimental data on hydrodynamics of the reactor, especially gas holdups and dispersion coefficients, are reported and discussed for the model studies with simulation and design of reactors.

2.2 Operating Conditions

The operating conditions and performances for the five runs covering seven major operating conditions with three kinds of coal, Tanitoharum (subbituminous coal), Adaro (low rank of subbituminous coal), and Ikeshima (low rank of bituminous coal) were reported by Ishibashi et al.5) and Hirano et al.6). In this study, the operations processing Tanitoharum coal were exclusively analyzed.

Table 2-1 shows the properties of the Tanitoharum coal which was processed in the plant.

Table 2-1. Properties of Tanitoharum Coal

Proximate analysis (dry coal basis)	
Volatile matter	47.0wt%
Fixed carbon	48.0wt%
Ash	5.0wt%
Moisture in feed coal	16.2wt%
Ultimate analysis, wt% daf basis	
C; 76.9 H; 5.8 N; 1.9 S; 0.15	
O(difference); 15.25	
Ultimate analysis of ash, wt% as oxide	
SiO_2; 27.7 Al_2O_3; 20.9 Fe_2O_3; 10.5	
MgO; 4.4 CaO; 12.9 P_2O_5; 1.4	
SO_3; 17.4 Na_2O; 3.0 Others; 1.8	

Table 2-2 shows the operating conditions of the four operation modes, as well as the data obtained on the pilot plant. These data are basically the average values for at least three days during the steady state period to obtain yield data. After allowing 9 days for start-up, the conditions of case 2 were maintained for 18 days, and the conditions of case 3 were maintained for 11 days. Finally, the coal concentration was increased to about 50 wt%, and the conditions for case 4 were maintained for 15 days. The recycle gas was fed into the reactors as a component of the feed and as the quench gas. The compositions of the recycle gas were slightly different for cases 1, 2 and 3. The flow rate of the recycle gas is given in units of volume (STP) per unit time and is denoted as G_r. At the feed line to the first reactor, G_r^a means the total flow rate of the gas injected before and after the preheater. The cold recycle gas is introduced to control the temperatures of the reactors, and the total flow rate of the recycle gas at the outlet of the third reactor increased to G_r^b. The slurry was a mixture of coal, recycle oil and powdered catalyst, the properties of which were shown in Table 2-3. The flow rate of the slurry is given in units of mass per unit time and is denoted as L_f. G_r^a/L_f and G_r^b/L_f as shown as the foot note of Table 2-2 are based on G_r^a and G_r^b, respectively. In case 1, which is referred to as "cold solvent operation," the recycle oil is fed to the reactor with the recycle gas at ambient temperature, before and after each coal liquefaction operation. Cases 2, 3, and 4 indicate the conditions of coal liquefaction processing Tanitoharum coal. The major difference between cases 2, 3, and 4 is the coal concentration in the feed slurry. Therefore, cases 2, 3, and 4 are hereafter referred to as "standard operation", "high concentration operation-1" and "high concentration operation-2," respectively.

In case 1, no temperature difference was detected between the bottom and the top of the reactor. In cases 2, 3, and 4, the heat was evoled by the reaction. The temperature at the top of the first reactor was controlled by introducing the quench gas within 20-30 K higher than that at the bottom. The feed temperature of the third reactor was approximately equal to the designed outlet temperature of the second reactor, and the temperature at the bottom of the third reactor was controlled at a few degrees lower than the temperature at the top of the third reactor, by adjusting the flow rate of the cold recycle gas, which was injected into the third reactor and the feed line to the third reactor. One possible reason for the temperature difference in the first reactor is the feed slurry temperature, which is lower than the temperature in the reactor. A lower temperature reduces the duty of the furnace. Another reason may be a small amount of backmixing in the reactor.

A total of 6 samples were withdrawn from the reactors during the operation in cases 2, 3, and 4, through nozzles (B) (middle) and (C) (bottom) of the first reactor, and a total of 6 samples through nozzle (B) of the second and third reactors during the operation.

Table 2-2. Operating conditions and data for the Kashima pilot plant

	case 1	case 2	case 3	case 4
Recycle gas				
Average molecular weight	2.1	5.48	5.71	5.78
Fraction of hydrogen, vol%	99	86	85	85
Makeup slurry				
Slurry feed rate, kg h^{-1}	7800	16200	15400	12700
Coal concentration in slurry, wt%, dry coal basis	0.0	40.0	43.7	48.5
Catalyst (pyrite powder) in slurry, wt%, dry coal basis	0	3	3	3
Reaction				
Operating pressure, MPa	16.6-16.8	→	→	→
Operating temperature,				
feed of the first reactor, K	313	673	671	664
bottom of the first reactor, K	313	699	709	713
top of the first reactor, K	313	728	733	733
feed of the second reactor, K	313	721	724	723
bottom of the second reactor, K	313	727	731	731
top of the second reactor, K	313	729	733	733
feed of the third reactor, K	313	724	729	728
bottom of the third reactor, K	313	726	731	731
top of the third reactor, K	313	728	733	733
G_r^a/L_f, m^3(STP)/kg-slurry*	3.38	0.55	0.55	0.71
G_r^b/L_f, m^3(STP)/kg-slurry**	3.38	0.71	0.70	0.90
Yields (daf coal basis), wt%				
In the liquefaction section				
Gas	0.0	17.2	20.0	20.4
Water	0.0	10.2	9.9	10.0
Oil (C4 to b.p. 811 K fraction)	0.0	51.0	53.1	55.6
Residue	0.0	26.1	21.6	18.8
Total	0.0	104.5	104.6	104.8
In the solvent hydrogenation section				
Gas	0.0	0.4	0.6	0.7
Water	0.0	0.7	1.3	1.3
Oil (C4 to b.p. 811 K fraction)	0.0	-0.3	-0.6	-0.7
Residue	0.0	0.0	0.0	0.0
Hydrogen consumption, wt%, dry ash free coal basis				
In the liquefaction section	0.0	4.5	4.6	4.8
In the solvent hydrogenation section	0.0	0.8	1.3	1.3

* (volumetric flow rate of recycle gas fed to the feed slurry)/(mass flow rate of makeup coal slurry)

** (volumetric flow rate of total recycle gas fed to the three reactors)/(mass flow rate of makeup coal slurry)

Table 2-3. Properties of liquefaction catalyst

Composition, wt%	Fe,	48.2
	S,	51.0
	Others,	0.8
Specific surface area, m^2 g^{-3}		6.1
Pulverized particle size (D50), µm		0.7-0.8

2.3 Physical Properties of the Gas and Slurry

The physical properties of coal liquids have been carefully determined in the EDS process[7] as well as the SRC-II process[8]. The results show that the physical properties of coal liquids are strongly dependent on liquefaction conditions and coal samples. As described above, a characteristic of the NEDOL Process is the downstream solvent hydrogenation section. The recycle oil, which was equilibrated after continuous operation of 1,000 h at the Kashima pilot plant, was fractionated into twelve narrow cuts by means of ASTM D 2829. The physical properties, such as boiling point (referred to herein as b.p.), vapor pressure, heat of vaporization, specific heat capacity, thermal conductivity, specific gravity and molecular weight, were then determined for each fraction. These data were stored in the reaction simulator, named Computer Aided Reactor Design, (CARD)[9], which is stated in Chapter 7 in detail. The Rackett equation[10] was used to correlate the temperature dependency of liquid density.

$$\rho = AB^{-\left[1+\left(1-T_r\right)^{2/7}\right]} \tag{1}$$

$$A = \frac{P_c}{RT_c}. \tag{2}$$

Constants, *A* and *B* were determined from the data measured in the range of 300-473 K, as shown in Table 2-4 [11]. All data relative to physical properties, including those of Tanitoharum coal itself, were stored in the process simulator, CARD[9]. The simulator also contained vapor-liquid equilibria and reaction rate coefficients of the coal and oil fractions, obtained at the Kashima pilot plant.

Table 2-5 shows the properties of the liquefied oil, which was fed to the solvent hydrogenation section, and the recycle oil, which was used to make the coal slurry. Although the composition of the recycle oil depends on liquefaction and hydrogenation conditions, the fraction of components having boiling points higher than 623 K reached approximately 35wt%, and that of aromatic compounds was higher than 50wt%. A part of the liquefied oil (several wt%) was discharged to the outside along with off-gas, waste water and residue.

When reaction conditions, such as flow rate, pressure and temperature, as well as the hydrodynamic characteristics of the reactor, such as gas holdup and axial dispersion coefficient, are known, the yields of gas and oil at the outlet of each reactor can be estimated from the simulator, CARD[9]. The vaporization of oil to the gas phase can also be estimated. Table 2-6 shows physical properties of the gas and slurry phases in the reactors. Considering the vaporization of light fractions of oil and production of gas and oil from coal and heavy oil and adjusting them with the pressure and temperature, the flow rates of gas of case 2 and 4 have been estimated under the liquefaction conditions.

Table 2-4. Constants for Rackett equation, A and B, for coal liquid fractions

fraction, K	normal boiling point, K	estimated critical temperature, K	A	B
IBP-423	356	541	0.2476	0.2445
423-453	439	647	0.2321	0.2114
453-473	465	688	0.2517	0.2212
473-493	485	714	0.2967	0.2634
493-513	505	736	0.2765	0.2441
513-533	525	758	0.2751	0.2432
533-553	547	784	0.2352	0.2022
553-573	568	809	0.2593	0.2230
573-593	588	832	0.2442	0.2069
593-613	608	856	0.2727	0.2320
613-633	630	885	0.2217	0.1809
633-653	651	911	0.2226	0.1774

Table 2-5. Properties of the recycle oil

	case 2		case 4	
	liq.*	hydrog.**	liq.*	hydrog.**
Ultimate Analysis				
C, wt%	87.19	87.40	87.91	88.61
H, wt%	9.53	9.99	9.29	10.04
N, wt%	0.97	0.82	1.08	0.61
S, wt%	0.03	0.02	0.02	0.01
O(difference), wt%	2.28	1.77	1.70	0.73
Specific gravity (288/277K)	1.004	0.991	1.008	0.983
PONA Analysis,wt%				
Parafin	20.1	20.5	19.6	19.8
Orefine	0.0	0.0	0.0	0.0
Naphthene	0.4	0.5	0.4	0.6
Aroma	58.2	57.5	56.6	50.4
Unidentified	21.3	21.5	23.5	29.2
Distillation (Gas Chromatographic distillation, ASTM D 2887), wt%				
473 K to 493 K	2.3	2.3	2.2	2.1
493 K to 533 K	16.6	16.9	14.6	15.5
533 K to 623 K	44.9	45.3	45.2	48.2
623 K to 723 K	32.5	31.9	32.4	29.6
723 K to 811 K	3.7	3.6	5.6	4.6

* feed oil to the hydrogenation section, referred to as liquefied recycle oil in Figure 1-1

** feed oil to the coal slurry preparation section after hydrogenation, referred to as hydrogenated recycle oil in Figure 1-1

Table 2-6. Physical properties used for the calculations

	case 1	case 2	case 4
[the first reactor]			
density of gas, kg m^{-3}	20	48	45
density of slurry, kg m^{-3}	964	730	790
viscosity of gas, m Pa s	0.01	0.02	0.02
viscosity of slurry, m Pa s	7.0	0.7	0.7
heat capacity of slurry, J kg^{-1} K^{-1}	-	2680	2680
thermal conductivity of slurry, W m^{-1} K^{-1}	-	0.163	0.174
average gas superficial velocity, m s^{-1}	0.063	0.056	0.058
average slurry superficial velocity, m s^{-1}	0.0031	0.0040	0.0027
gas holdup, -	0.53	0.47	0.49
[the third reactor]			
density of gas, kg m^{-3}		62	
density of slurry, kg m^{-3}		730	
viscosity of gas, m Pa s		0.02	
viscosity of slurry, m Pa s		0.4	
heat capacity of slurry, J kg^{-1} K^{-1}		2760	
thermal conductivity of slurry, W m^{-1} K^{-1}		0.140	
average gas superficial velocity, m s^{-1}		0.071	
average slurry superficial velocity, m s^{-1}		0.0033	
gas holdup		0.55	

2.4 Gas Holdup

The most important factor affecting the reactor volume or the actual residence time for reaction is gas holdup, ε_g, which is dependent on mainly gas and liquid superficial velocities, physical properties of both fluid, gas distributor, existence of particles, and dimensions of columns. The effect of pressure on the gas holdup has been investigated in small-size columns up to 0.23 m in diameter for gas-liquid systems by Wilkinson et al.[12)], Lin et al.[13)], and Letzel et al.[14)] for gas-slurry systems by Kojima et al.[15)] at extremely high pressures (up to 20 MPa) by Luo et al.[16)] These results show that pressure increase leads to a higher gas holdup up to 0.5-0.6. Since in the field of coal liquefaction, gas holdups were measured in the liquefaction reactors of Exxon Donor Solvent Process, Exxon Coal Liquefaction Plant (EDS, ECLP) (0.61 m in diameter)[3)], Solvent Refined Coal-II Process, Ft. Lewis Plant (SRC-II) (0.61 m in diameter)[17)], Brown Coal Liquefaction Process, Victoria Plant (BCL) (0.60 m in diameter)[19)], and the Interessen Gemeinschaft, Bottrop Plant (IG) (1.2 m in diameter)[18)] with tracers and differential pressures. Under the conditions of NEDOL process, Takeshita et al.[20)] proposed the correlation based on 0.13 m and 0.24 m-diameter reactors. Moreover, Mochizuki et al.[21)] reported the gas holdup data up to 0.03 m s^{-1} of gas superficial velocity in Process Supporting Unit (PSU) reactors of NEDOL process (0.175 m in diameter). Since all the effects of the chemical, physical, mechanical, and geometrical factors affecting the gas holdup were not quantitatively clarified, the data obtained under the coal liquefaction conditions in a larger column were required to design a large-scale reactor of NEDOL process.

The author et al.[22,23)] measured the gas holdup in the Kashima pilot plant reactors, using the following two methods.

(1) A differential pressure method at hot-oil (673 K) and coal liquefaction conditions.

(2) A gas shutdown method at cold-oil conditions.

ΔP between two positions with a vertical distance of L is expressed by

$$\Delta P = \left\{ \rho_l \left(1 - \varepsilon_g \right) + \rho_g \varepsilon_g \right\} g L \qquad (3)$$

where ρ_l and ρ_g are the densities of liquid and gas phases and ε_g is the gas holdup. The gas holdup, ε_g, was explicitly calculated from the static pressures between pressure gauges (A) and (C), ΔP, shown in Figure 1-4 by the following equation.

$$\varepsilon_g = \frac{\left\{ 1 - \dfrac{\Delta P}{\rho_l g L} \right\}}{\left\{ 1 - \left(\dfrac{\rho_g}{\rho_l} \right) \right\}} \qquad (4)$$

Under the coal liquefaction conditions, ρ_l is replaced by the density of slurry, ρ_{sl}, which was estimated by CARD[9)].

The second method, a gas shutdown method, was taken once to determine the gas holdup with a hydrogen-oil system at ambient temperature and at 16.9 MPa. When hydrogen gas and oil were steadily fed to the first reactor, the gas was instantaneously stopped. The gas and liquid phases were naturally separated in the reactor. Then, the oil was fed to the reactor until the liquid level reached the top of the reactor. The gas holdup was calculated from the volume of additional feed of oil and the reactor volume.

Figure 2-1 shows the experimental gas holdup data not only in the Kashima plant reactors, but also those in the coal liquefaction pilot and small-plant reactors, which include Recycle Coal Liquefaction Unit (RCLU) (0.024 m in diameter) and Coal Liquefaction Pilot Plant (CLPP) (0.066 m in diameter) reactors of EDS process.

The author et al.[22)] found that the data obtained in the Kashima pilot plant were in agreement with the correlation proposed by Tarmy et al.[3)] for U_g = 0.02-0.07 m s^{-1}.

$$\frac{U_g}{\varepsilon_g} = (U_g + U_{sl}) + U_b (1 - \varepsilon_g)^m \qquad (5)$$

where U_b = 0.09 m s^{-1} and m = 0.65. Equation (5) was used in the calculation in the study. The estimated curve with U_{sl}= 0.003 m

s^{-1} shown in Figure 2-1 matched the data of BCL as well, but the deviation between the data of the Kashima pilot plant reactor and the curve increased in the range of 0.07-0.08 m s^{-1}. Then, Ishibashi and the author et al. [23)] proposed that U_g = 0.114 m s^{-1} and m = 1.02 as shown as a thin line in Figure 2-1.

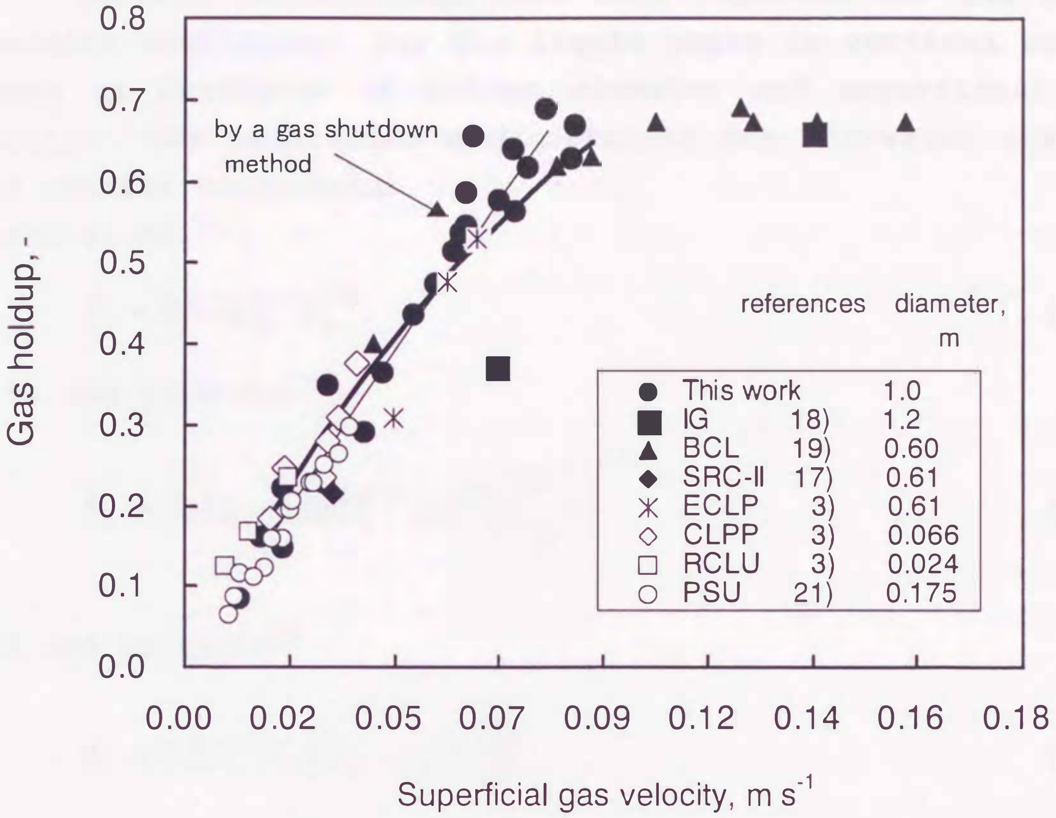

Figure 2-1. Effect of superficial gas velocity on gas holdup in various liquefaction reactors. Thick line, estimated by Equation (5) with U_g=0.09 m s^{-1}, m=0.65; thin line, estimated by Equation (5) with U_g=0.114 m s^{-1}, m=1.02. (Ishibashi and the author et al.[23])

2.5 Dispersion Coefficient

Several correlations have been reported for the axial dispersion coefficient for the liquid phase in vertical bubble columns as functions of column diameter and superficial gas velocity. The majorities were obtained for air-water systems under ambient conditions.

Deckwer et al.24):

$$E_l = 0.678 D_t^{1.4} U_g^{0.3} \tag{6}$$

Hikita and Kikukawa25):

$$E_l = (0.15 + 0.69 U_g^{0.77}) D_t^{1.25} \left(\frac{10^{-3}}{\mu_l} \right)^{0.12} \tag{7}$$

Field and Davidson26):

$$E_l = 0.9 D_t^{1.5} \left[L_s \left(U_g - \varepsilon_g U_s \right) \right]^{\frac{1}{3}} \tag{8}$$

Kato and Nishiwaki27):

$$\frac{U_g D_t}{E_l} = \frac{13 Fr}{1 + 6.5 Fr^{0.8}} \tag{9}$$

$$Fr = \frac{U_g}{\left(g D_t \right)^{0.5}} \tag{10}$$

where E_l is the axial dispersion coefficient, D_t the column diameter, L_s the submerged length from the free surface, and U_s the slip velocity. In Equations (6)-(10), it is necessary to express all quantities in the SI base units; i.e., kg-m-s systems.

In coal liquefaction reactors, however, liquid dispersion coefficients, as determined by tracer tests, were found to be smaller than those estimated from the above correlations3,19,29).

Singh et al.[29)] also reported that the axial dispersion coefficient, estimated from temperature profiles in the reactor (0.61 m i.d., 10 m length) at the Fort Lewis SRC-II plant, was approximately 1/3 of the value obtained from Equation (6). Morooka et al.[30)] measured gas holdups and liquid dispersion coefficients for air-water systems and evaluated the effect of a surfactant dissolved in water. When polyoxyethylene-p-iso-octylphenyl ether was added at a concentration of 100 ppm, the dispersion coefficient was decreased to less than 1/10 of the value without the surfactant.

A neutron absorption tracer technique (NAT) was applied to the Kashima plant by Sakai and the author et al.[31)] A tracer slurry was prepared by suspending the gadolinium powder in the recycle oil at a concentration of 50 wt%. Approximately 0.05-0.06 m^3 of the slurry was injected into the feed line to the first or third reactor within 15 s. At the vertical exit line from the first or third reactor, low energy neutrons were irradiated using californium-252 as the neutron source. The injection and detection points are shown in Figure 1-3. Neutrons were counted using a ^{3}He-filled proportional counter, which was installed at the opposite side of the pipe from the neutron source, and the neutron intensity was converted to the concentration of the tracer. The residence time distribution curves of the first and third reactors were obtained in several cases, including cases 1, 2, and 4 as shown in Table 2-2. But, the average operating conditions for few hours during the measurement were slightly different from those for several days shown in Table 2-2. Table 2-7 shows only different data from those. Thus, in the present study, "standard operation" is denoted as case 2' and "high concentration operation-2" as case 4' as distinguished the data shown in Table 2-2.

Table 2-7. Operating conditions for neutron absorption tracer technique

	case 1	case 2'	case 4'
Slurry feed rate, kg h^{-1}	7800	15600	12400
$G_r/L_f{}^*$, m^3(STP)/kg-slurry	3.38	0.59	0.80
$G_r/L_f{}^{**}$, m^3(STP)/kg-slurry	3.38	0.75	0.96

* (volumetric flow rate of recycle gas fed to the feed slurry)/(mass flow rate of makeup coal slurry)

** (volumetric flow rate of total recycle gas fed to the three reactors)/(mass flow rate of makeup coal slurry)

When the reactor is modeled as a closed vessel, the first and the second moments of the residence time distribution curve are related to the mean residence time, τ, and the axial dispersion coefficient, E_1, respectively[32).

$$\tau = \frac{\sum tc(t)}{\sum c(t)} \tag{11}$$

$$\sigma_t^2 = \frac{\sum t^2 c(t)}{\sum c(t)} - \tau^2 \tag{12}$$

$$\sigma^2 = \frac{\sigma_\tau^2}{\tau^2} = \frac{2}{Pe} - 2\frac{\left[1 - \exp(-Pe)\right]}{Pe^2} \tag{13}$$

$$E_l = \frac{L\left[\dfrac{u_l}{1-\varepsilon_g}\right]}{Pe} \tag{14}$$

$$N = \frac{1}{\sigma^2} \qquad (15)$$

where L is the length of the reactor, which is 11.8 m in length in the present case, σ^2 is the variance, and N is the equivalent number of completely stirred tanks in series.

Figures 2-2 shows normalized residence time distribution curves, c/c_0, in cases 1, 2', and 4' in the first reactor and case 2' in the third reactor. From Equation (14), the axial dispersion coefficients of the liquid phase in the first and third reactors were determined to be 0.11 $m^2\ s^{-1}$ and 0.13 $m^2\ s^{-1}$ for the cold oil operation, 0.029 $m^2\ s^{-1}$ and 0.039 $m^2\ s^{-1}$ for the standard liquefaction operation, 0.022 $m^2\ s^{-1}$ and 0.028 $m^2\ s^{-1}$ for the high concentration liquefaction operation-2, respectively. The mean residence time of the liquid phase was also determined for each run as shown in Table 2-8.

Figure 2-3 shows the data of the axial dispersion coefficients of the liquid phase obtained in this study. The data reported by Tarmy et al.[3)] and Tanaka et al.[19)] in the range of U_g = 0.04-0.08 m s^{-1} are also plotted in the figure. These literature data were obtained in the coal liquefaction reactors (0.60-0.61 m i.d.). The axial dispersion coefficients, which were measured in this study under the liquefaction conditions, are one order of magnitude smaller than those calculated from Equations (6) and (9) for air-water system at ambient pressure and temperature and 1/3-1/6 of those obtained for the cold oil.

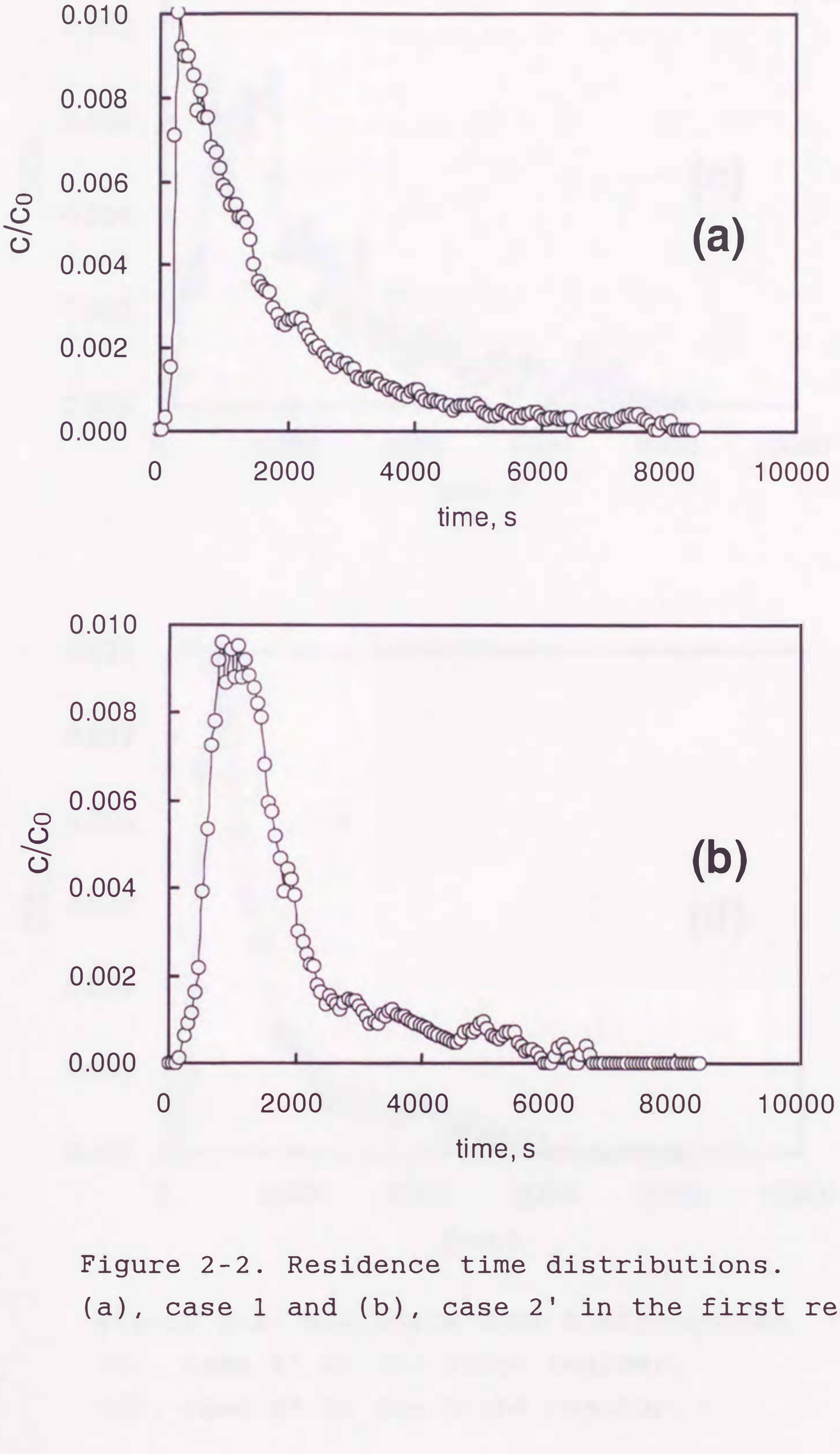

Figure 2-2. Residence time distributions.
(a), case 1 and (b), case 2' in the first reactor.

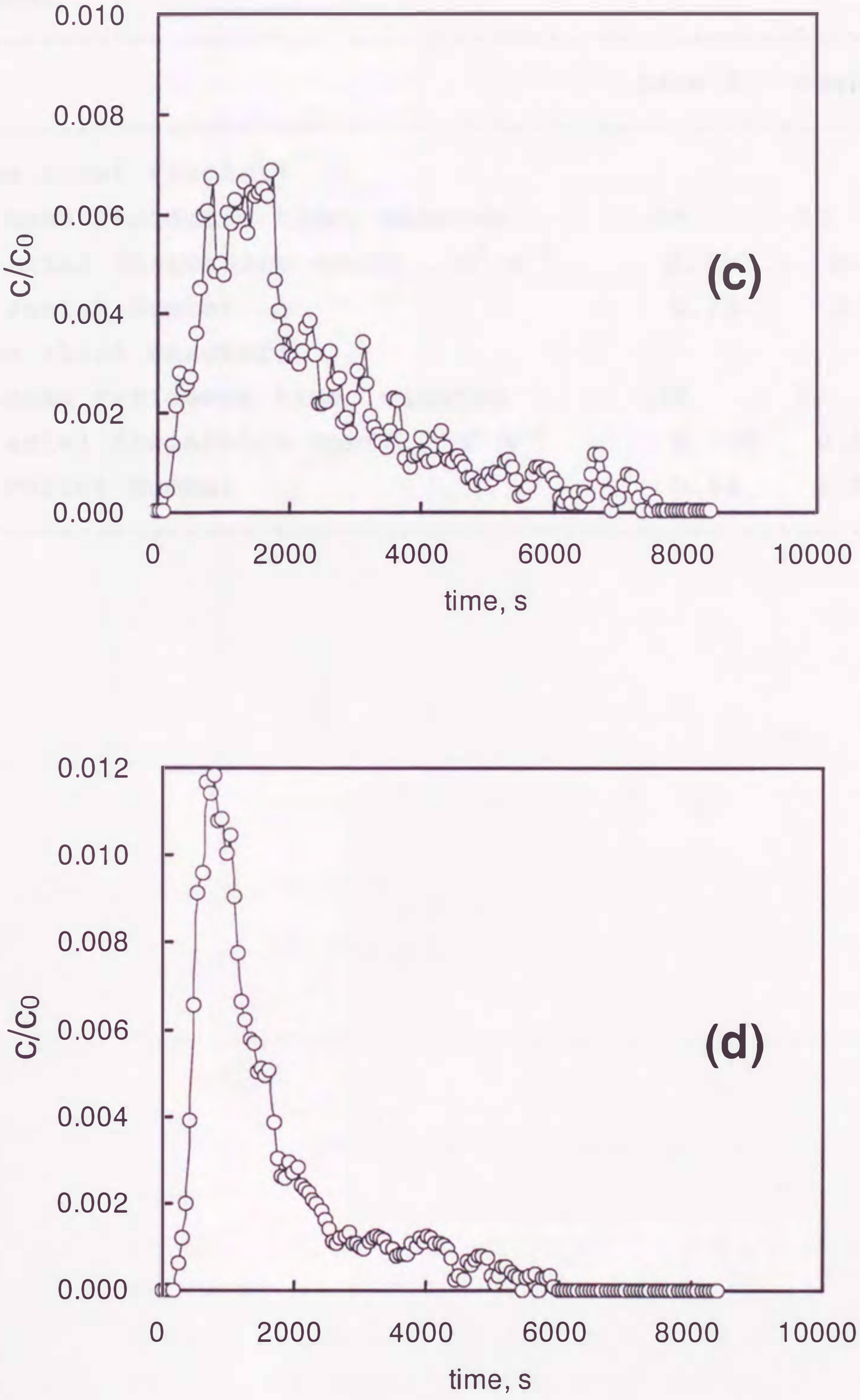

Figure 2-2. Residence time distributions.
(c), case 4' in the first reactor;
(d), case 2' in the third reactor.

Table 2-8. Measured axial dispersion coefficients and Peclet Number

	case 1	case 2'	case 4'
[the first reactor]			
mean residence time, minutes	29	30	38
axial dispersion coeff., m^2 s^{-1}	0.110	0.029	0.022
Peclet Number	0.73	2.7	2.7
[the third reactor]			
mean residence time, minutes	28	27	35
axial dispersion coeff., m^2 s^{-1}	0.130	0.039	0.029
Peclet Number	0.66	2.2	2.3

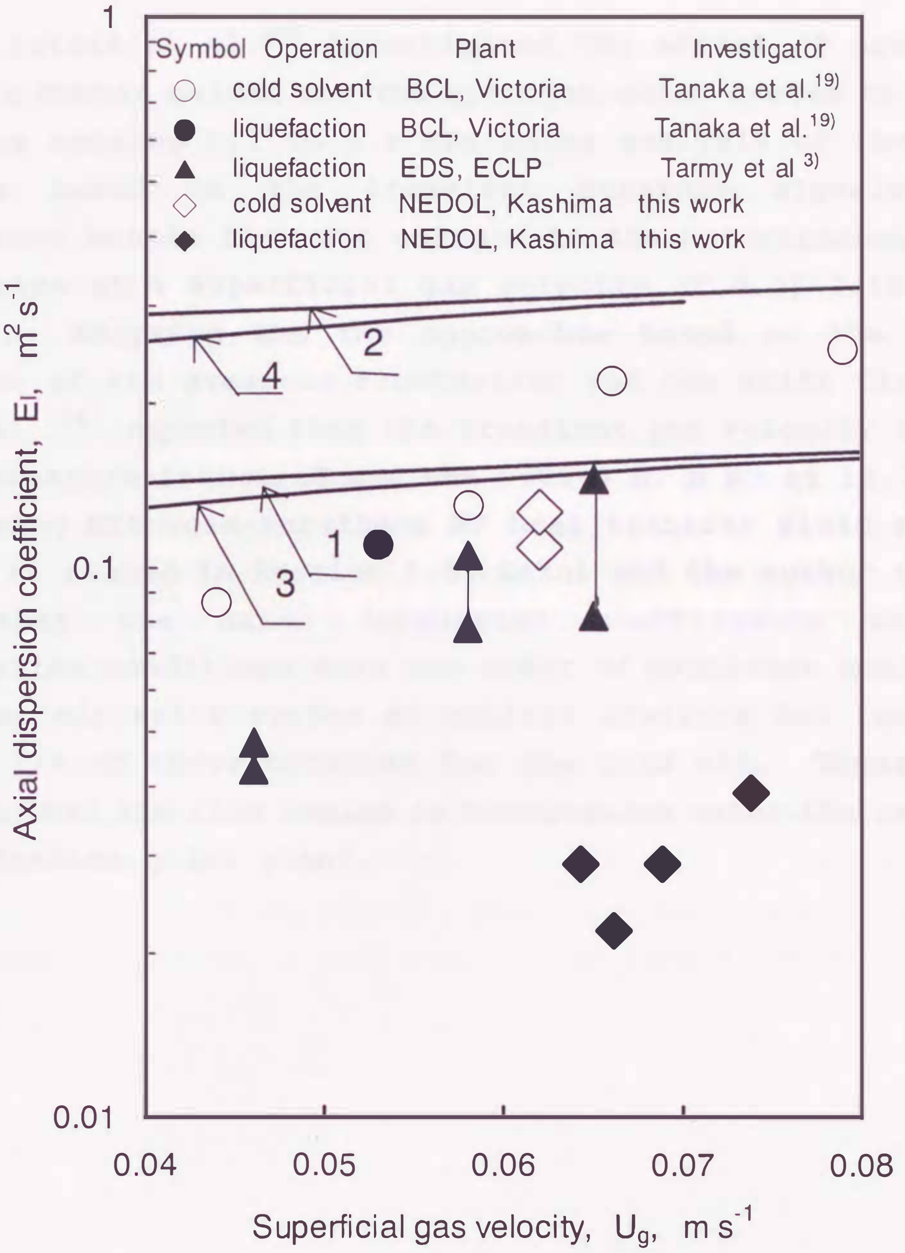

Figure 2-3. Effect of superficial gas velocity of axial dispersion coefficients.
Line 1, Equation (9) for D_t = 0.61 m;
line 2, Equation (9) for D_t = 1.0 m;
line 3, Equation (6) for D_t = 0.61 m;
line 4, Equation (6) for D_t = 1.0 m.
(Sakai and the author et al. [31])

2.6 Flow Regime

Letzel et al.[33)] investigated the effect of pressure on flow in a bubble column for the nitrogen-water system at elevated pressures ranging 0.1 to 0.9 MPa using analysis of the chaotic features based on the transient pressure signals. The homogeneous bubble flow was changed to the heterogeneous bubbly flow regime at a superficial gas velocity of 0.08-0.10 m s^{-1} at 0.9 MPa. Adopting the two approaches based on the standard deviation of the pressure fluctuation and the drift flux model, Lin et al. [34)] reported that the transient gas velocity increased as the pressure increased and was 0.06-0.07 m s^{-1} at 15.2 MPa and 351 K using Nitrogen-Paratherm NF heat transfer fluid system.

As stated in Section 2.5, Sakai and the author et al. [31)] found that the axial dispersion coefficients under the liquefaction conditions were one order of magnitude smaller than those for air-water system at ambient pressure and temperature and 1/3-1/6 of those obtained for the cold oil. These results indicate that the flow regime is homogeneous under the conditions of the Kashima pilot plant.

2.7 Conclusions

In this chapter, the common information used for analyses of the Kashima pilot plant and discussion for a large-scale reactors were described. Especially, the followings are concluded on the gas holdup and dispersion coefficients, major factors characterizing the hydrodynamics of the liquefaction reactors, by the data obtained through the operation.

(1) Using the reaction simulator, CARD, the flow rates and physical properties in the reactors were predicted.

(2) The data obtained in the Kashima pilot plant were in agreement with the correlation proposed by Tarmy et al.[3)], which was based on the data in the liquefaction reactors of EDS Process. The effect of diameter on the gas holdup was not found in the range of 0.175-1.0 m of diameter within 0.07 m s^{-1} of a superficial gas velocity.

(3) The axial dispersion coefficients under the liquefaction conditions measured by a neutron absorption tracer technique were one order of magnitude smaller than those for air-water system at ambient pressure and temperature and 1/3-1/6 of those obtained for the cold oil. These results indicate that the flow regime is homogeneous under the conditions of the Kashima pilot plant.

Nomenclature

c = concentration, kg m^{-3}

c_0 = initial concentration, kg m^{-3}

E_l, E_{sl} = dispersion coefficients of liquid and slurry phases, respectively, m^2 s^{-1}

D_t = diameter of reactor, m

Fr = Fruid Number

G_q = volumetric flow rate of quench gas, m^3(STP) s^{-1}

G_r = volumetric flow rate of recycle gas, excluding gas and oil vapor which are evolved by reactions, m^3(STP) s^{-1}

g = gravity acceleration, m s^{-2}

L = length, m

L_f = makeup slurry flow rate, kg h^{-1}

L_s = submerged length from the free surface, m

N = equivalent number of completely stirred tanks, -

P = pressure, MPa

P_c = critical pressure, K

Pe = Peclet Number, -

T = temperature, K

T_c = critical temperature, K

T_r = reduced temperature, -

U_g, U_l, U_{sl} = superficial velocity of gas, liquid, and slurry, respectively, m s^{-1}

U_s = slip velocity, m s^{-1}

ΔP = pressure drop, kPa

ε_g = gas holdup

μ_l = viscosity of liquid, kg m s^{-1}

ρ_g, ρ_{sl} = density of gas and slurry, respectively, kg m^{-3}

σ^2 = variance, -

τ = mean residence time, s

Subscripts

f = quantity in the feed line to the first reactor

g = gas phase

l = liquid phase

sl = slurry phase

References

(1) Fan, L.S.; Tsuchiya, K. *Bubble wake dynamics in liquids and liquid-solid suspensions*; Butterworth-Heinemann: Stoneham, MA, 1990.

(2) Deckwer, W.D. *Bubble column reactors;* Wiley: Chickester, England, 1992.

(3) Tarmy, B.L.; Chang, M.; Coulaloglou, C. A.; Ponzi, P. R. The three phase hydrodynamics of the EDS coal liquefaction reactors: their development and use in reactor scaleup. *Inst. Chem. Eng., Sym. Ser.* **1984**, No.87, 303-317.

(4) Fan, L.S.; Yang, G.Q.; Lee, D.L.; Tsuchiya, K.; Luo, X. Some aspects of high-pressure phenomena of bubbles in liquids and liquid-solid suspensions. *Chemical Engineering Science* **1999**, *54*, 4681-4709.

(5) Ishibashi, H.; Kouzu, M.; Hayashi, T.; Kamei, T.; Oi, S.; Endo, M. et al. Study for development of the coal liquefaction process by 150 t/d coal liquefaction pilot plant (I) -Operational technology and effect of reaction conditions on product yields-. *J. Japan Inst. Energy*, **1998**, *77*, 1201-1213.

(6) Hirano, K. Outline of NEDOL coal liquefaction process development -Pilot plant program-. *J. Japan Inst. Energy*, **1999**, *78*, 845-851.

(7) Tsonopoulos, C.; Heideman, J.L.; Hwang, S.C. Thermodynamic and transport properties of coal liquid, An Exxon Monograph, John Wiley & Sons, New York, 1986.

(8) Gray, J.A.; Brady, C.J.; Cunningham, J.R.; Freeman, J.R.; Wilson, G.M. *Ind. Eng. Chem. Process Des. Dev.* **1983**, *22*, 410-424.

(9) Hiraide, M.; Itoh, H.; Kidoguchi, A.; Kaneda, E.; Kobayashi, M.; Namiki, Y.; Imada, Y.; Inokuchi, K. Coal liquefaction reactor simulator. *Proc. Int. Symp. Fundamentals for Innovative Coal Utilization, Sapporo*, **1999**, 103-106.

(10) Rackett, H.G. Equation of state for saturated liquids. *Journal of Chemical Engineering Data*, **1970**, *15*, 514-517.

(11) Oneyama, M.; Koyama, K.; Sato, H.; Aramaki, T.; Hayashi, T.; Kobayashi, M. Physical property correlation of coal liquids. *Proc. 35th Coal Science Conf., Tsukuba* **1998**, No.61.

(12) Wilkinson, P.T.; Spek, A.P.; van Dierendonck, L.L. Design parameters estimation for scale-up of high-pressure bubble columns. *AIChE J.* **1992**, *38*, 544-554.

(13) Lin, T.J.; Tsuchiya, K.; Fan, L.S. Bubble flow characteristics in bubble columns at elevated pressure and temperature. *AIChE J.* **1998**, *44*, 545-560.

(14) Letzel, H.M.; Schouten, J.C.; Krishna, R.; Bleek, C.M. van den Gas holdup and mass transfer in bubble column reactors operated at elevated pressure. *Chemical Engineering Science* **1999**, *54,* 2237-2246.

(15) Kojima, H.; Okumura, B.; Nakamura, A. Effect of pressure on gas holdup in a bubble column and a slurry bubble column. *Journal of Chemical Engineering of Japan*, 24,115-117.

(16) Luo, X.L.; Lee, D.J.; Lau, R.; Yang, G.; Fan, L.S. Maximum stable bubble size and gas holdup in high-presure slurry bubble columns. *AIChE J.* **1999**, *45*, 665-680.

(17) Pittsburg & Midway Coal Mining Co. *Solvent Refined Coal (SRC) Process, Final report, DOE/ET/*10104-46; 1982.

(18) Kürten, H. Verfahrenstechnik der kohlehydrierung in sumpfphasen-reaktoren. *Chem. Ing. Tech.* **1982**, *54*, 409-415.

(19) Tanaka, Y.; Tamura, M.; Kageyama, H.; Clark, K. Fluid dynamics studies in the brown coal liquefaction reactor. *2nd Japan/Australia Joint Technical Meeting on Coal, Tokyo*, **1992**, 198-204.

(20) Takeshita, M.; Takayasu, M.; Fukuyama, M.; Sakai, N.; Ueda, S.; Yoshida, H.; Yokoyama, K.; Hayashi, T. Gas hold-up equation for suspended bubble column reactor of coal liquefaction. *1989 Intern. Conf. Coal Sci., Tokyo,* **1989,** 859-863.

(21) Mochizuki, M.; Imada, K.; Ikeda, K.; Inokuchi, K.; Nogami, Y.; Takeda, T.; Sakawaki, K. Study of fluid dynamics in coal liquefaction reactor. *4th Japan/German Symp. On Bubble Columns, Kyoto,* **1997**, 393-400.

(22) Onozaki, M.; Ishibashi, H.; Namiki, Y.; Takagi, T.; Kobayashi, M. Gas hold-up of bubble column coal liquefaction reactor of 1 m Diameter. *Proc. 63rd Annual Meeting of Chem. Eng.* **1998,** Osaka, Japan.

(23) Ishibashi, H.; Onozaki, M.; Kobayashi, M.; Hayashi, J.; Itoh, H.; Chiba, T. Gas holdup in slurry bubble column reactors of a 150 t/d coal liquefaction pilot plant. *Fuel Processing Technology*, submitted.

(24) Deckwer, W.D.; Burckhart, R.; Zoll, G. Mixing and mass transfer in tall bubble columns. *Chemical Engineering Science* **1974**, *29*, 2177-2188.

(25) Hikita, H.; Kikukawa, H. Liquid-phase mixing in bubble columns: Effect of liquid properties. *Chem. Eng. J.* **1974**, *8*, 191-197.

(26) Field, R. W.; Davidson, J. F. Axial dispersion in bubble column. *Trans IchemE* **1980**, *58*, 228-236.

(27) Kato, Y.; Nishiwaki, A. Longitudinal dispersion

coefficient of liquid in bubble column. Kagaku Kogaku **1971**, *35*, 912.

(28) Panvelker, S. V.; Tierney, J. W.; Shah, Y. T.; Rhodes, D. F. Backmixing in a SRC dissolver. *Chemical Engineering Science* **1982**, *37*, 1582-1585.

(29) Singh, C.P.P.; Carr, N. L. Liquefaction of coal by SRC-II Process Part IV: Steady-state thermal behavior of the reactor. *Can. J. Chem. Eng.* **1982,** *60*, 831-841.

(30) Morooka, S.; Mizoguchi, T.; Kago, t.; Kato, Y.; Hidaka, N. Effect of fine bubbles on flow properties in bubble column with suspended solid particles. *J. Chem. Eng. Japan* **1986**, *19*, 507-512.

(31) Sakai, N.; Onozaki, M.; Saegusa, H.; Ishibashi, H.; Hayashi, T.; Kobayashi, T.; Tachikawa, N.; Ishikawa, I.; Morooka, S. Characterization of fluid dynamics in coal liquefaction reactors using Neutron Absorption Tracer Technique. *AIChE J.* **1999**, submitted.

(32) Levenspiel, O. *Chemical Reaction Engineering*; John Wiley & Sons: New York, 1962.

(33) Letzel, H.M.; Schouten, J.C.; Bleek, van den C. M.; Krishna, R. Influence of elevated pressure on the stability of bubbly flows. *Chemical Engineering Science* **1997**, *52*, 3733-3739.

(34) Lin, T.J.; Tsuchiya, K.; Fan, L.S. **1999,** On the measurements of regime transition in high-pressure bubble columns. *The Canadian Journal of Chemical Engineering*, *77*, 370-374.

3. Steady-State Thermal Behavior of Coal Liquefaction Reactors

3.1 Introduction

The temperature at the top of each reactor was maintained at a designated value by adjusting the flow rate of cold recycle gas (quench gas), which was introduced into the reactor at different heights. In the first reactor, the temperature at the bottom was 20-30 K lower than that at the top. In the second and third reactors, however, the temperature at the bottom was nearly equal to that at the top. One reason for the temperature difference in the first reactor is that the feed slurry temperature is lower than the temperature in the reactor and is determined so as to increase the thermal efficiency of the preheating section. Having the feed at a lower temperature reduces the duty of the furnace for preheating. Another reason may be the small backmixing in the reactor. The hydrodynamic behaviors of the coal liquefaction reactors in Exxon Donor Solvent Process (EDS), Solvent Refined Coal-II Process (SRC-II), and Brown Coal Liquefaction Process (BCL) pilot plants were studied with tracer[1-3)], and the results showed that liquid-phase axial dispersion coefficients in the reactors were smaller than those obtained in bubble columns for air-water systems operated at ambient pressure and temperature.

In order to establish the steady-state operation of liquefaction plants, design items, such as the feed temperature, the locations of quench gas injection, the amount of quench gas, and the hydrodynamics in coal liquefiers, need to be more fully examined. Singh et al.[4)] analyzed temperature profiles in the reactor at the Fort Lewis SRC-II plant. However, their data are not directly applicable to other reactors. Thus, the objective of this study[5)] is to develop a reactor model, which can be generally utilized in the design and operation of large-scale coal liquefaction reactors, which will be constructed in the future.

3.2 Axial Dispersion Model

The reactant, which is defined as the organic fraction of the coal in the present study, is converted to gas and oil by consuming hydrogen. The heat, which is generated via hydrogenation, is transferred downstream and is partially lost to the surroundings through the reactor and pipe walls. At the injection points for the quench gas, the temperature decreases discontinuously in a manner which satisfies the local heat balance.

The following assumptions are made:

(a) Temperature and reactant concentration are uniform horizontally.

(b) The oil consists of components whose boiling points are higher than C_4 hydrocarbons and lower than 811 K.

(c) The slurry, which is a mixture of oil, coal and catalyst, is assumed to be a homogeneous fluid. The coal consists of the reactive component (reactant) which is hydrogenated to gas and oil, the inertinite fraction which is organic in nature but inert to liquefaction, and, finally, the inorganic mineral matter. When the slurry is heated, a portion is vaporized to the gas phase. The vaporization ratio is defined as the ratio of the mass which is vaporized to the gas phase in each reactor to the mass of the slurry at the top of the reactor. The mass flow rate of the slurry is decreased, and that of the gas phase is increased, as a result of the vaporization. The gas phase, which includes hydrogen, hydrocarbons and other inorganic gases, undergoes volume and density changes as the results of factors, such as the temperature rise along the axial position, the evolution of gas by liquefaction, the vaporization of oil, and the introduction of the quench gas at the quenching positions.

(d) The heat of reaction is proportional to the amount of hydrogen consumed[6,7]. The heat of reaction generated in each reactor is calculated, based on the hydrogen consumption in the corresponding reactor. The reaction rate is dependent on the concentration of the reactant and is independent of hydrogen pressure and temperature. The latter assumption is valid in the narrow range of reaction conditions adopted in this pilot plant.

(e) The heat loss through the walls of reactors and connecting tubes is proportional to the temperature difference between the wall and the prevailing atmosphere, and is calculated using the thermal conductivity and thickness of the insulator.

(f) The gas holdup, ε_g, is dependent on superficial gas velocity, U_g, and superficial slurry velocity, U_{sl}. The axial dispersion coefficient of the slurry, E_{sl}, is dependent on the superficial gas velocity.

(g) The axial dispersion coefficient of heat is equal to that of the slurry.

The differential equation with respect to reactant concentration in the reactors, c, can then be described as follows:

$$E_{sl}(1-\varepsilon_g)\frac{d^2c}{dx^2} - U_{sl}\frac{dc}{dx} + R_{cV} = 0 \tag{1}$$

where x is the axial coordinate, and R_{cv} is the reaction rate of coal based on the reactor volume. The reaction rate, which is based on the slurry volume, R_c, is given as

$$R_c = \frac{R_{cV}}{(1-\varepsilon_g)} \tag{2}$$

The hydrogen consumption rate, based on the reactor volume, R_{hv}, is given by the following equation.

$$R_{hV} = \frac{R_{cV}}{r_{hc}} \tag{3}$$

where r_{hc} is the ratio of the consumed reactant mass to the consumed hydrogen mass.

The temperature in the reactors, T, is expressed as

$$E_{sl}(1-\varepsilon_g)H_{mix}\frac{d^2T}{dx^2} - U_{sl}H_{mix}\frac{dT}{dx} + (\Delta HR_{hV} - H_{loss} - H_q) = 0 \tag{4}$$

where H_{mix} is the heat capacity of the mixture of gas and slurry and is calculated from

$$H_{mix} = \frac{\rho_g Cp_g U_g}{U_{sl}} + \rho_{sl}Cp_{sl} \tag{5}$$

ΔH is the heat of reaction based on the rate of hydrogen consumption, and H_{loss} is the heat loss to the atmosphere. H_q is the cooling rate by the quench gas, and $H_q = 0$ except for the positions of the injection nozzle. The boundary conditions of the outlet of the reactor are given by

$$\text{At } x = L_t;\ T = T_{out},\ c = c_{out},\ dT/dx = 0,\ dc/dx= 0 \qquad (6)$$

where L_t is the effective reactor height, including the bottom and top sections ($L_t = 11.8$ m). T_{out} and c_{out} are given as the fixed conditions for each run. At the quench gas nozzles, the rate of heat removal is given by

$$H_q = (T - T_q)Cp_q\rho_q \qquad (7)$$

where T_q and ρ_q are the temperature and density of the quench gas, respectively.

Equations (1) and (4) are numerically integrated from the outlet to the inlet, and the iteration is continued until the calculated feed concentration and temperature, c_f and T_f, agree with the data. In Equation (8), c_{out} is related to the concentration of the reactant at the bottom of the first reactor, c_f.

$$c_f = c_{out}[1 - (\text{ratio of vaporization})] + (\text{c decreased by reaction}) \qquad (8)$$

$$T_f = T_{out} - [(\text{heat of reaction}) - (\text{heat of vaporization}) - (\text{heat removed by quench gas}) - (\text{heat loss to circumstance})]/[(\text{heat capacity of slurry}) + (\text{heat capacity of recycle gas})] \qquad (9)$$

Similar equations are also derived for the second and third reactors.

3.3 Model Parameters

3.3.1 Operating Conditions

In the present study, "standard operation" (case 2) and "high concentration operation-2" (case 4) of Tanitoharum coal were principally adopted for simulation. Adding concentrations of components used for the simulation in this chapter to Table 2-2, the operating conditions are shown in Table 3-1.

3.3.2 Gas Holdup

Equation (5) in Section 2.4 was used in the present study.

3.3.3 Axial Dispersion Coefficient

The axial dispersion coefficient of the slurry phase is expressed by modifying Equation (5) of Section 2.5 as follows:

$$E_{sl} = f_D U_g^{0.3} \tag{10}$$

where f_D is the correlation factor, and E_{sl} and U_g are in units of $m^2 s^{-1}$ and $m\ s^{-1}$, respectively. f_D is determined by a simulation, which is described in the later section.

Table 3-1. Operating conditions and data for the Kashima pilot plant

	Case 2	Case 4
Coal, dry coal basis		
Mineral matters in coal, wt%,	5	5
Inertinite in coal, wt%	5	5
Recycle gas		
Average molecular weight	5.48	5.78
Fraction of hydrogen, vol%	86	85
Makeup slurry		
Recycle oil feed rate, kg h^{-1}	9540	6340
Coal feed rate, dry coal basis, kg h^{-1}	6480	6180
Slurry feed rate, kg h^{-1}	16200	12700
Coal concentration in slurry, wt%, dry coal basis	40	48.5
Catalyst (pyrite powder) in slurry, wt%, dry coal basis	3	3
Reactant concentration in slurry, kg m^{-3}-slurry	260	340
Reaction		
Operating pressure, MPa	16.6-16.8	16.6-16.8
Operating temperature at the top of the first reactor, K	728	733
$G_r/L_f{}^*$, m^3(STP) kg^{-1}-slurry	0.55	0.71
$G_r/L_f{}^{**}$, m^3(STP) kg^{-1}-slurry	0.71	0.90
Evaporation ratio at the feed line to the first reactor	0.18	0.18
Reactant concentration at the feed line with evaporation, kg m^{-3}-slurry	317	415
Results at the outlet from the third reactor		
Reactant concentration without evaporation, kg m^{-3}-slurry	55	49
Gas fraction, wt%, dry coal basis	26	29
Oil fraction, wt%, dry coal basis	49	53
Unreacted reactant, wt%, dry coal basis	19	13
Yields (daf coal basis), wt%		
Gas	17.2	20.4
Water	10.2	9.9
Oil (C_4 to b.p. 811 K fraction)	51.0	55.6
Residue	26.1	18.8
Total	104.5	104.8
Hydrogen consumption (daf coal basis), wt%	4.5	4.8

*(volumetric flow rate of recycle gas fed to the feed slurry)/(mass flow rate of makeup coal slurry)

**(volumetric flow rate of total recycle gas fed to the three reactors)/(mass flow rate of makeup coal slurry)

3.3.4 Physical Properties of Gas and Slurry

As mentioned in Section 2.3, the flow rates and the physical properties are calculated by the reaction simulator, CARD.

3.3.5 Heat Loss

From the overall enthalpy balance between the inlet flow of the first reactor and the outlet flow of the third reactor, the total heat loss of the three reactors and connecting pipes was calculated to be 6.14×10^5 kJ h^{-1}. The heat loss due to all connecting pipes was calculated to be 0.86×10^5 kJ h^{-1}. The heat loss from the wall of each reactor was then calculated to be 1.76×10^5 kJ h^{-1}, by subtracting the heat loss due to pipes from the total heat loss and by dividing the resulting heat loss into three parts.

3.3.6 Heat of Reaction

Table 3-2 shows the heat balances in the reactors, as calculated from Equation (9) using the simulator. A part of the oil fraction is vaporized. The vaporization ratios, which are calculated based on vapor-liquid equilibria stored in the simulator, are also shown in Table 3-2. The temperature and G_r/L_f in the outlet line from one reactor were not identical to the values in the inlet line to the next reactor. A small amount of recycle gas, which was injected into the connecting line between the reactors, as well as the heat loss, contributed to the temperature drop in the connecting line.

The overall heat of reaction per 1 m^3 (STP) of consumed hydrogen was 2090 kJ for case 1 and 2180 kJ for case 2. The fractions of the heat of reaction generated in the first, second, and third reactors were, respectively, 0.64, 0.23 and 0.13 in case 2 and 0.68, 0.21 and 0.11 in case 4. Singh et al.[8)] reported that the heat of reaction was 2120 kJ m^{-3}(STP)-hydrogen. This value was derived from the data obtained in the P-99 pilot plant reactor, in conjunction with the SRC-II process, where the hydrogen consumption was 4.4 wt% of the dry ash free coal. Ohshima et al.[6)] used a hot-walled stirred tank reactor, which was operated continuously, and determined the heat of reaction for Canadian Battle River coal to be 2140 kJ m^{-3}(STP)-hydrogen. The values obtained in the present study are in agreement with these reported values.

Table 3-2. Heat balances around the liquefaction reactors

	First reactor	Second reactor	Third reactor	Total
[Case 2; standard operation]				
Temperature at the inlet line, K	678	721	724	
Temperature at the outlet line, K	782	729	728	
$(G_r/L_f)^a$ measured at the bottom, m^3 kg^{-1}	0.55	0.60	0.68	
$(G_r/L_f)^a$ measured at the top, m^3 kg^{-1}	0.58	0.67	0.71	
Vaporization ratio at the reactor outlet	0.52	0.56	0.60	
Enthalpy difference between outlet and inlet, MJ h^{-1}				
Sensible heat of vaporized slurry	284	133	75	492
Latent heat of vaporized slurry	827	97	97	1021
Sensible heat of remaining slurry	1809	170	85	2064
Sensible heat of recycle gas	787	133	83	1003
Heat loss to circumstances	176	176	176	528
Cooling by quench gas	301	768	295	1364
Heat of reaction, kJ m^{-3}(STP)-hydrogen				2180
Heat generated in reactor, MJ h^{-1}	4184	1478	810	6473
Fraction of heat generated in reactor	0.64	0.23	0.13	1.0
[Case 4; high concentration operation-2]				
Temperature at the inlet, K	664	723	728	
Temperature at the outlet, K	733	733	733	
$(G_r/L_f)^*$ measured at the bottom m^3 kg^{-1}	0.71	0.78	0.86	
$(G_r/L_f)^*$ measured at the top, m^3 kg^{-1}	0.76	0.86	0.90	
vaporization ratio at the reactor outlet	0.62	0.68	0.73	
Enthalpy difference between outlet and inlet, MJ h^{-1}				
Sensible heat of vaporized slurry	270	141	72	483
Latent heat of evaporation	816	103	103	1022
Sensible heat of remaining slurry	1812	121	49	1983
Sensible heat of recycle gas	1089	167	86	1342
Heat Loss to circumstances	176	176	176	528
Cooling by quench gas	391	711	233	1335
Heat of reaction, kJ m^{-3}(STP)-hydrogen				2090
Heat generated in reactor, MJ h^{-1}	4554	1419	719	6693
Fraction of heat generated in reactor	0.68	0.21	0.11	1.0

[*] (volumetric flow rate of recycle gas fed into each reactor)/ (mass flow rate of makeup coal slurry)

3.3.7 Reaction Rate

Since reaction models which assume multiple hydrogenation and decomposition pathways are too complex for the simulation of temperature profiles in the reactors. Thus the reactant is assumed to be a single component in the present study. The amount of the unreacted reactant is defined as

(reactant, kg) = (coal, kg) - (mineral matters, kg) -
(inert coal, kg) - [(produced gas and oil, kg) -
(consumed hydrogen, kg)] (11)

where the amount of hydrogen which is transferred to gas and oil from the gas phase is subtracted from the total produced amount of gas and oil, resulting in the net amount of gas and oil which are formed from the reactant. The inert component of coal is defined as the inertinite fraction. The reactant concentration, c, is defined as

(reactant concentration, kg m^{-3}) =
(reactant, kg)/(slurry volume, m^{3}) (12)

In case 2, the coal concentration in the makeup slurry is 40 wt%, and the slurry density is 730 kg m^{-3}, as shown in Table 3-2. Since no vaporization of oil occurs for the makeup slurry, the reactant concentration in 1 m^{3} of the makeup slurry can be calculated from Equation (11) and is found to be (1-0.05-0.05)x 0.40x730 = 260 kg m^{-3} on the dry coal basis. The total yield of gas and oil at the outlet of the third reactor is 0.26+0.49 = 0.75. Thus c at the outlet of the third reactor is calculated from equations (11) and (12) to be (1-0.05-0.05-0.26-0.49+0.04) x0.40x730 = 55 kg m^{-3}, assuming that all oil vapor is condensed in the slurry phase. For case 4, c in the makeup slurry and at the outlet from the third reactor is 340 and 49 kg m^{-3}, respectively, as shown in Table 3-1. However, the vaporization of oil from the heated slurry phase needs to be taken into consideration in calculating the reactant concentration in the reactors from Equation (1). The vaporization ratio in each reactor is calculated from the vapor-liquid equilibria and is listed in Table 3-1. The vaporization of oil results in a decrease in the slurry volume, and, as a result, the reactant concentration is increased. For case 2, the heated slurry in the feed line to the first reactor is partially vaporized with a vaporization ratio of 0.18. Thus c is calculated to be 260/(1-0.18) = 317 kg m^{-3}. The evaporation proceeds further in the first reactor, the temperature of which is high.

Wiser[9)] reported that 94 wt% of the total leachable components in coal were produced in the initial dissolution stage via a kinetically second-order reaction with respect to the reactant concentration and that the reaction gradually became first-order kinetics in the later stages. Thus, the following equation can be applied to the reaction in the first reactor.

$$R_c = kc^2 \tag{13}$$

The reaction kinetics in the second and third reactors may be different from those described by Equation (13). For simplicity, however, the same kinetics is applied to the reaction in the second and third reactors, the contribution of which is not great, in comparison to the first reactor. The activation energy for the reaction is assumed to be zero in the narrow temperature range considered in the present study. The reaction rate coefficient, k, for case 2 can then be estimated by the following procedure:

(i) The reaction rate coefficient is assumed so as to satisfy the reactant concentrations in the feed line to the first reactor and the outlet line from the third reactor;

(ii) the ratio of reactant consumption rate to hydrogen consumption rate, r_{hc}, is determined so that the heat generation due to the calculated total hydrogen consumption is balanced to the total heat of reaction obtained in the overall series of reactors; and

(iii) the heat of reaction in each reactor is calculated and compared to the value which is calculated from the heat balance obtained experimentally from the temperatures and flow rates between the inlet and outlet of the respective reactor.

This procedure is repeated until step (iii) is satisfied. The vaporization ratios, as well as the physical properties of the gas and slurry phases, are estimated using the simulator. The axial dispersion coefficient of the slurry is also determined. Thus the value of k is obtained as follows:

$$k = 7.87\times10^{-7}\ \text{m}^3\text{-slurry kg}^{-1}\text{-reactant s}^{-1} \qquad (14)$$

The reaction rate in Equation (1) is then calculated as

$$R_{cv} = 7.87\times10^{-7}c^2(1 - \varepsilon_g)\ \text{kg-reactant m}^{-3}\text{-reactor s}^{-1} \qquad (15)$$

The hydrogen consumption ratio is calculated as

$$r_{hc} = 14\ \text{kg-reactant/kg-hydrogen} \qquad (16)$$

As shown in Figure 3-1, the pressure difference between the inlet (D) and the outlet (A) of the first reactor, P(D) - P(A), gradually increased by 11 kPa after 280 h of operation, although the operating conditions of case 2 remained unchanged. After the reactor was further operated for one month under the conditions of case 3, the operation of case 4 was initiated. The pressure difference, P(D) - P(A), was further increased by 40 kPa as the result of the operation of case 4 and reached 102 kPa (not shown in Figure 3-1). It has been reported by Morooka et al.[10)] that calcium and magnesium carbonates are deposited in liquefaction reactors. In the NEDOL Process, the fine pyrite powder, which was used as the catalyst, acted as nucleation sites and presumably enhanced the deposition of mineral particles. Solid particles were sampled from the first reactor, and the average density of these was determined to be 2700 kg m^{-3}. It was estimated that approximately 18 % of the first reactor volume was comprised of solid particles in the operation of case 4. Since no severe scales were found on the wall of the reactors by inspection after the operation, it is probable that the solid particles were fluidized in the first reactor during the operation. The analysis of this phenomena is stated in Chapters 5 and 6 in detail. Thus, the reaction rate coefficient, which is defined on the basis of the original reaction volume, should be decreased by 18 % in case 4. The dispersion coefficient in case 4 is assumed to be equal to that in case 4, irrespective of the presence of solid particles.

Figure 3-1 also shows the time-dependent changes in temperature differences between thermometer (A) and thermometers (B)-(E) in the first reactor in case 2. At 80 h after the startup, the flow rate of the quench gas was increased for 20 h. Although thermometers (B)-(E) were installed at evenly spaced intervals, the temperature difference between (C) and (D) increased gradually, along with an increase in pressure difference. This supports the view that the solid particles caused a decrease in heat generation per unit reactor volume in the lower part of the first reactor.

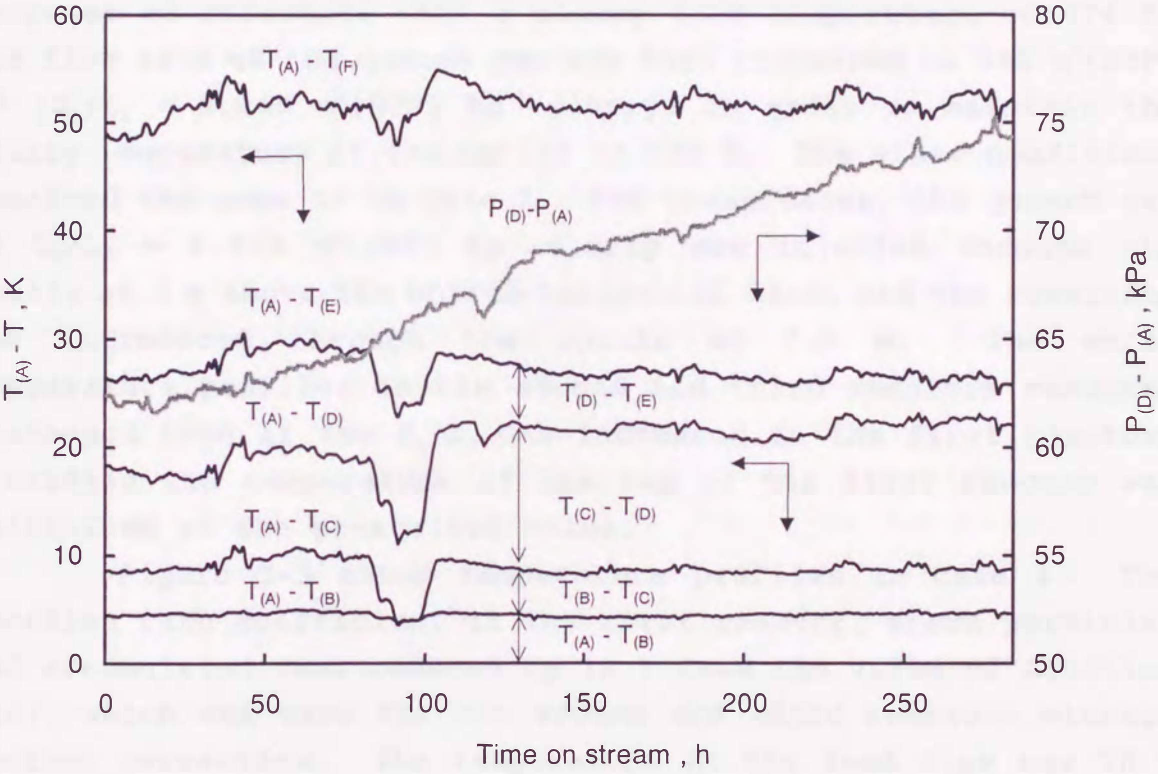

Figure 3-1. Temperature and pressure differences in the first reactor.

3.4 Results and Discussion

Figure 3-2 shows the temperature profiles in case 2 for two flow rates of quench gas fed to the first reactor. The standard temperature at the top of the reactor was fixed at 728 K. In the standard run, the volumetric flow rate of quench gas was 370 m^3(STP) h^{-1}, and the ratio of the flow rate of the quench gas to that of the makeup slurry, (G_q/L_f), was 0.024 m^3(STP) kg^{-1}-slurry. The temperature of the slurry at the inlet line of the first reactor was 672 K. The other run was carried out for purposes of reference with a slurry feed temperature of 676 K. The flow rate of the quench gas was then increased to 940 m^3(STP) h^{-1} (G_q/L_f = 0.060 m^3(STP) kg^{-1}-slurry) in order to maintain the slurry temperature at the outlet at 728 K. The other conditions remained the same as in case 2. For these cases, the quench gas of G_q/L_f = 0.012 m^3(STP) kg^{-1}-slurry was injected through the nozzle at 4 m above the bottom tangential line, and the remainder was introduced through the nozzle at 7.5 m. The axial temperature profiles in the second and third reactors remained unchanged even if the G_q/L_f was increased in the first reactor, providing the temperature at the top of the first reactor was maintained at the prescribed value.

Figure 3-3 shows temperature profiles in case 4. The reaction rate coefficient in the first reactor, where particles had accumulated, was reduced by 18 % from the value of Equation (14), which was used for the second and third reactors without further correction. The temperature at the feed line was 70 K lower than that at the top of the reactor. Since the top temperature of the first reactor was maintained at 733 K in case 4, the temperatures at all axial positions were higher than those in case 2. The large difference in temperatures at the bottom and top of the first reactor can be attributed to the higher generation of the heat of reaction in case 4, where a higher concentration slurry was fed.

The dispersion coefficient of the slurry phase was determined to be 0.03-0.04 m^2 s^{-1} for cases 2 and 4 and was in the range shown in Table 2-8. This value was 0.13 times that of

Equation (6) in Section 2.5, i.e., $f_D = 0.088$ in Equation (10). In the present study, the axial dispersion coefficient for heat is assumed to be equal to that for the reactant in the slurry phase as described in assumption (g). However, the axial dispersion of heat is more complex than the dispersion of reactants, since gas bubbles ascend at a much higher velocity than the slurry and contribute to the axial transfer of heat under high pressures. Thus it is desirable to estimate the axial dispersion coefficient of heat from axial temperature profiles in the reactor. This remains a subject for future studies.

Table 3-3 shows the results of the calculation as well as the data obtained in the pilot plant. The estimated fraction of the heat generation in each reactor is in good agreement with the calculation based on the heat balances for both cases 2 and 4. The reactant concentration without evaporation at the outlet of the third reactor for case 2 is 55 kg m^{-3}-slurry as shown in Table 3-1, and is in good agreement with the calculated value (53 kg m^{-3}-slurry) shown in Table 3-3. For case 2, the experimental and calculated values are, respectively, 49 and 30 kg m^{-3}-slurry. This discrepancy can be attributed to the reaction rate coefficient, k, which was determined for case 2 and then applied to case 4. The correction based on the accumulation of solid particles in the first reactor for case 4 was insufficient. In general, however, the model developed in the present study is sufficient to calculate thermal behaviors of liquefaction reactors operated under different conditions.

Table 3-3. Results of thermal simulation

	First reactor	Second reactor	Third reactor
[Case 2; standard operation]			
Physical properties			
Density of gas, kg m^{-3}	48	59	62
Density of slurry, kg m^{-3}	730	730	730
Heat capacity of gas, kJ $(kg\ K)^{-1}$	3.31	3.27	3.18
Heat capacity of slurry, kJ $(kg\ K)^{-1}$	2.68	2.80	2.76
Calc. superficial velocity of gas, m s^{-1}	0.056	0.065	0.071
Calc. superficial velocity of slurry, m s^{-1}	0.004	0.0036	0.0033
Calc. gas holdup	0.47	0.52	0.56
Calc. reactant concentration at the reactor bottom with vaporization, kg m^{-3}	393	237	163
Calc. reactant concentration at the reactor outlet with vaporization, kg m^{-3}	271	181	132
Calc. reactant concentration at the reactor outlet without vaporization, kg m^{-3}	130	80	53
Fraction of heat generated in reactor			
Experimental	0.64	0.23	0.13
Calculated	0.62	0.25	0.13
[Case 4; high concentration operation-2]			
Physical properties			
Density of gas, kg m^{-3}	45	57	60
Density of slurry, kg m^{-3}	790	790	790
Heat capacity of gas, kJ $(kg\ K)^{-1}$	3.31	3.27	3.22
Heat capacity of slurry, kJ $(kg\ K)^{-1}$	2.68	2.76	2.80
Calc. superficial velocity of gas, m s^{-1}	0.058	0.066	0.071
Calc. superficial velocity of slurry, m s^{-1}	0.0027	0.0020	0.0017
Calc. gas holdup	0.49	0.54	0.57
Calc. reactant concentration at the reactor bottom with vaporization, kg m^{-3}	473	235	139
Calc. reactant concentration at the reactor outlet with vaporization, kg m^{-3}	311	170	110
Calc. reactant concentration at the reactor outlet without vaporization, kg m^{-3}	118	56	30
Fraction of heat generated in reactor			
Experimental	0.68	0.21	0.11
Calculated	0.68	0.23	0.09

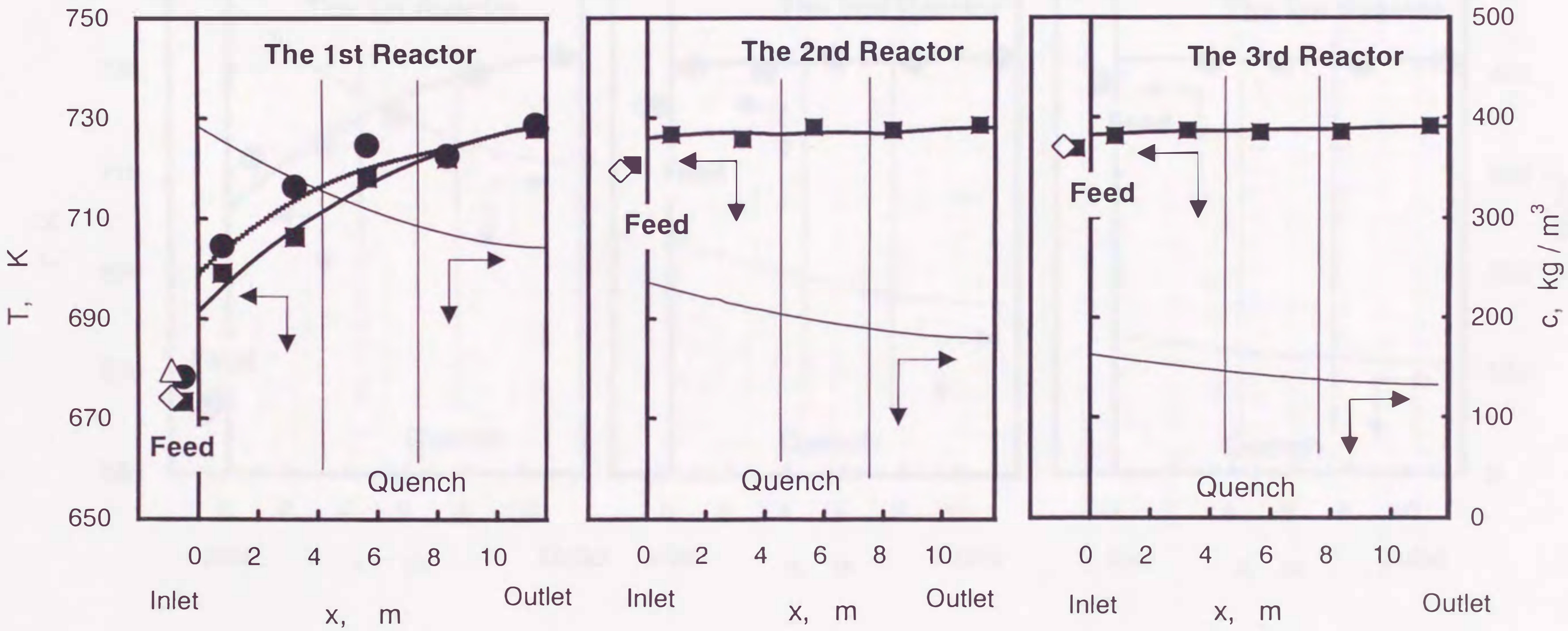

Figure 3-2 Temperature profiles in reactors (case2).
Solid lines and ◇, calculation for G_q/L_f = 0.024 m^3(STP) kg^{-1}-slurry;
broken lines and △, calculation for G_q/L_f = 0.060 m^3(STP) kg^{-1}-slurry;
■ and ●, experiment for G_q/L_f = 0.024 and 0.060 m^3(STP) kg^{-1}-slurry, respectively.

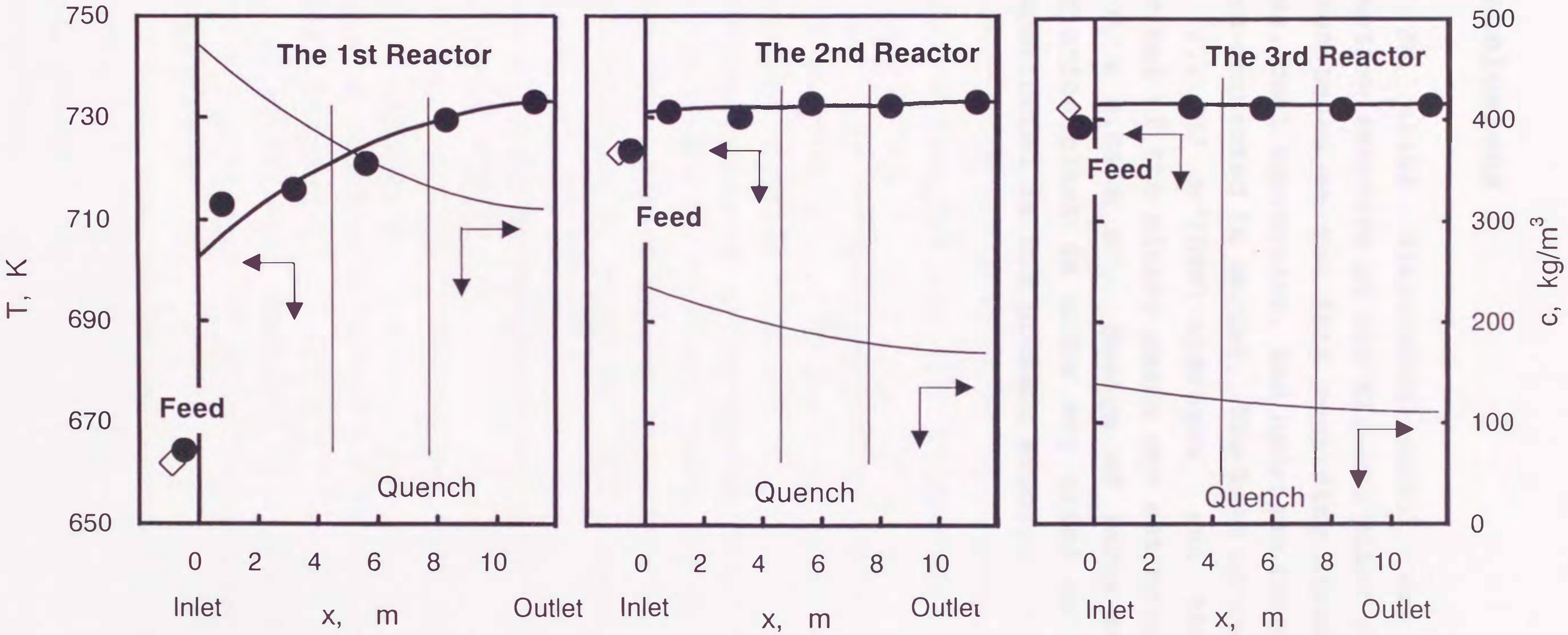

Figure 3-3. Temperature profiles in reactors (case 4).
Solid lines and ◇, calculation; ●, experiment.

3.5 Conclusions

An axial dispersion model was applied to coal liquefaction reactors at the Kashima pilot plant. The model was validated based on the data regarding steady-state temperature profiles, coal conversion, and hydrogen consumption in the three reactors connected in series. The heat of reaction was estimated to be 2.1 MJ m^{-3}(STP)-hydrogen, and the axial dispersion coefficient of the slurry phase was estimated to be 0.03-0.04 m^2 s^{-1} at U_g = 0.06 m s^{-1}. Design of large-scale reactors for a demonstration plant is under way based on the model which has been constructed in the present study.

Nomenclature

C_{pg}, C_{pq}, C_{psl} = specific heat capacity of gas including oil vapor, quench gas, and slurry, respectively, J $(kg\ K)^{-1}$

c = concentration of reactant in slurry phase, respectively, kg m^{-3}-slurry

E_l, E_{sl} = dispersion coefficients of liquid and slurry phases, $m^2\ s^{-1}$

D_t = diameter of reactor, m

f_D = correlation factor of equation (10)

G_q = volumetric flow rate of quench gas, m^3(STP) s^{-1}

G_r = volumetric flow rate of recycle gas, excluding gas and oil vapor which are evolved by reactions, m^3(STP) s^{-1}

ΔH = heat of reaction per mass of hydrogen consumed, J kg^{-1}-hydrogen

H_{loss} = heat loss per unit volume of reactor, J m^{-3}-reactor s^{-1}

H_q = heat removed by quench gas injection per unit volume of reactor, J m^{-3}-reactor s^{-1}

H_{mix} = heat capacity of gas-slurry mixture, J m^{-3}-slurry K^{-1}

k = reaction rate coefficient, m^3-slurry kg^{-1}-reactant s^{-1}

L_f = mass flow rate of makeup slurry, kg s^{-1}

L_t = effective length based on volume including top and bottom parts, m

R_c = rate of reactant converted per unit volume of slurry, kg m^{-3}-slurry s^{-1}

R_{cv} = rate of reactant converted per unit volume of reactor, kg m^{-3}-reactor s^{-1}

R_{hv} = rate of hydrogen consumed per unit volume of reactor, kg m^{-3}-reactor s^{-1}

r_{hc} = ratio of reactant consumed to hydrogen consumed, kg kg^{-1}

T, T_f, T_q = temperature of reactor, feed and quench gas, respectively, K

U_g, U_{sl} = superficial velocity of gas and slurry, respectively, m s^{-1}

x = axial position, m

ε_g = gas holdup

ρ_g , ρ_q , ρ_{sl} = density of gas including oil vapor, quench gas, and slurry, respectively, kg m^{-3}

Subscripts

f = quantity in the feed line to the first reactor

g = gas phase

l = liquid phase

out = quantity in the outlet line from the third reactor

q = quench gas

sl = slurry phase

References

(1) Tarmy, B.L.; Chang, M.; Coulaloglou, C. A.; Ponzi, P. R. The three phase hydrodynamics of the EDS coal liquefaction reactors: their development and use in reactor scaleup. *Inst. Chem. Eng., Sym. Ser.* **1984**, No.87, 303.

(2) Panvelker, S. V.; Tierney, J. W.; Shah, Y. T.; Rhodes, D. F. Backmixing in a SRC dissolver. *Chemical Engineering Science* **1982**, *37*, 1582-1585.

(3) Tanaka, Y.; Tamura, M.; Kageyama, H.; Clark, K. Fluid dynamics studies in the brown coal liquefation reactor. *2nd Japan/Australia Joint Technical Meeting on Coal, Tokyo*, **1992**, 198-204.

(4) Singh, C.P.P.; Carr, N. L. Liquefaction of coal by SRC-II Process Part IV: Steady-state thermal behavior of the reactor. *The Canadian Journal of Chemical Engineering* **1982**, *60*, 831-841.

(5) Onozaki, M.; Namiki, Y.; Ishibashi, H.; Takagi, T.; Kobayashi, M.; Morooka, S. Thermal-steady state behavior of coal liquefaction reactors. *Energy & Fuels* **2000**, in press.

(6) Ohshima, S.; Suzuki, M.; Shimada, K.; Yumura, M.; Takematsu, T.; Kuriki, Y.; Yoshitome, H. Characteristics of a laboratory scale C.S.T. reactor and their effect on coal liquefaction. *Kagaku Kogaku Ronbunshu* **1984**, *10*, 483-488.

(7) Ueda, S.; Yokoyama, S.; Ishii, T.; Makino, K.; Takeya, G. The heat of hydrodesulfurization reaction of heavy oil. *I&EC Process Design and Development* **1975**, *14*, 493-499.

(8) Singh, C.P.P.; Carr, N. L. Liquefaction of coal by SRC-II Process Part IV: Steady-state thermal behavior of the reactor. *The Canadian Journal of Chemical Engineering* **1982**, *60*, 831-841.

(9) Wiser, W. H. A kinetic comparison of coal pyrolysis and coal dissolution. *Fuel* **1968**, *47*, 475-486.

(10) Morooka, S.; Kato, Y.; Ikejiri, S.; Nakajima, M.; Matsuyama, H. Preliminary simulation of ash accumulation in dissolver of direct coal liquefaction. *J. Chem. Eng. Japan* **1986**, *19*, 137-139.

4. Dynamic Simulation of Gas-Liquid Dispersion Behavior in Coal Liquefaction Reactors

4.1 Introduction

The hydrodynamic behaviors of coal liquefaction reactors are significantly different from those obtained in bubble columns for air-water systems, operated under ambient pressure and temperature as stated in Section 2. However, the empirical approach used in the previous studies may not be applicable to coal liquefaction reactors with large dimensions. In order to design reactors which are 2-5 m in diameter, gas-liquid flow under conditions of coal liquefaction has to be expressed by proper modeling.

Freedman and Davidson1) developed a flow model for bubble columns based on liquid circulation, and Joshi and Sharma2) proposed a model, which consisted of multiple circulation cells. Recently, Degaleesan et al.3) developed a more complex, two-compartment convective-diffusion model. Degaleesan and Dudukovic4) developed a relationship between axial dispersion coefficients and convective recirculation, as well as eddy diffusion.

A two-fluid Eulerian model involving turbulent energy is often applied to simulate fluid dynamics in bubble columns5-10). Recent advances in computer technology have enabled the application of Eulerian-Lagrangian models to unsteady-state dynamics in bubble columns11-17). In these models, the volume-averaged Navier-Stokes equation was used to describe hydrodynamics of the liquid phase, and the equation of motion was used to track each spherical bubble. The role of solid particles in three-phase (gas-liquid-solid) bubble columns was also investigated for bubble dynamics by Majumdar et al.18,19). In the churn-turbulent regime, three phases consisting of liquid, small bubbles, and large bubbles was implemented within the Eulerian framework by Krishna et al.20).

However, all previous studies have been performed for the case of air-water systems under ambient conditions. No simulations of hydrodynamics have been reported in two- and three-phase bubble column reactors, which are operated at elevated pressures and temperatures for coal liquefaction.

Thus, the objective of this study[21)] is to determine whether a dynamic model based on an Eulerian-Lagrangian approach for bubble flows has the capability of predicting residence time distributions of the slurry phase under coal liquefaction conditions. The residence time distribution curves, as well as the axial dispersion coefficients, were predicted by the simulation and compared with the experimental data. The hydrodynamic model developed in the present study be used to design large-scale coal liquefaction reactors, which are to be constructed in the future.

4.2 Fluid Dynamical Model

Lapin and Lübbert[12)] modeled the gas-liquid two-phase flow using Navier-Stokes equations in a Eulerian representation for liquid phase. Bubbles were individually tracked through the homogeneous liquid in a Lagrangian way. Delnoij et al.[14)] developed a conjugated Eulerian-Lagrangian approach, in which bubble-bubble interactions were expressed by an collision model. In the present study, the liquid phase is described using the volume averaged Navier-Stokes equation, and the gas phase is described by the equations of motion for an individual bubble. The k-ε model which was proposed for the turbulence stresses by Kato and Launder[22)], referred to as the MP k-ε model, is applied to the reactors to precisely predict the turbulent flow pattern even at stagnation points. The dynamic simulation was carried out using a commercial CFD code "Stream" (Copyright; Software Cradle Co.) using an engineering work station. A pseudo-three-dimensional model was used to obtain residence time distributions using a finite-volume solution algorithm. To reduce the calculation time the following assumptions were made:

(a) The slurry phase in the liquefaction reactor is a homogeneous liquid. Particles of coal ash and pyrite catalyst are smaller than the size of the computation grids. Sedimentation and growth of particles do not occur.

(b) A cylindrical coordinate is applied. The liquefaction reactor, which is 1 m in diameter, is sliced with a vertical plane including the central axis into a wedge with an angle of 0.05 radians.

(c) The hydrodynamics in bubble columns at elevated pressures, i.e., 16.6-16.8 MPa in coal liquefaction, can be characterized by smaller and more stable bubbles than those at ambient conditions for air-water systems[23)]. Luo et al.[24)] reported that size distributions of bubbles were narrower at elevated pressures (5.6 MPa). In the present study, a superficial gas velocity was assumed to be less than 0.07 m s^{-1} to maintain the homogeneous bubble flow as mentioned in Section 2.5. Thus, all bubbles are assumed to be spherical and to have an identical diameter with no breakup or coalescence. The slip velocity to the radial direction is assumed to be zero.

(d) In the liquefaction reactors, the gas holdup is in the range of the maximum values, 0.5-0.6, as a homogeneous bubble flow [25]. Thus the variation of the gas holdup along the vertical and radial directions is neglected.

(e) Neither mass transfer nor phase change occurs between the gas and liquid phases. The compositions in the gas and liquid phases are assumed to be constant. The flow rates and physical properties of the gas and liquid phases are estimated using a process simulator, and the averaged values are applied. Only the flow rate of the liquid phase can be determined by the tracer test data. The flow rates of the gas and liquid phases vary along the vertical direction due to the reactions in the reactors. The predicted gas flow rates at the inlet and outlet of the reactors, as well as the average value are listed in Table 2-2.

(f) In the cold solvent operation, the temperature in the reactor is uniform. In the liquefaction operation, however, the temperature distribution in the reactor may cause a buoyant force in the liquid phase. Heat generated per unit volume is constant in the reactor.

(g) A fraction of the generated heat is lost through the vertical wall of the reactor at a constant rate.

(h) The cold recycle gas is introduced into the reactor through two nozzles, which is open along the central axis of the reactor as shown in Figure 1-3. The heat removed is assumed to be a half of the generated heat in the reactor.

(i) Bubble-bubble interactions are neglected.

(j) The log-law[26] is applied to the turbulent flow near the wall as follow:

$$\frac{u(y)}{u^*} = \frac{1}{\kappa}\ln\frac{u^* y}{\nu} + A \qquad (1)$$

$$u^* = \sqrt{\frac{\tau_0}{\rho}} \qquad (2)$$

where u(y) is the velocity of fluid, u* the friction velocity expressed by Equation (2), κ (=0.4) Karman constant, y the vertical distance from the boundary, ν kinematic viscosity, A (=5.5) the constant, τ_0 the shear stress.

Bubble dynamics: The trajectory of a bubble is calculated from the absolute bubble velocity vector, $\mathbf{u}_b$, which is defined as follows:

$$\mathbf{u}_b = \mathbf{u}_l + \mathbf{u}_{slip}. \tag{3}$$

At a steady state, the slip velocity of a bubble is equal to that of an isolated bubble without any interaction among the bubbles. Since no reliable equation is available under high pressures and temperatures, however, the steady-state slip velocity of bubbles is assumed a priori based on the gas holdup. At an unsteady state, the major forces acting on the bubble are gravity, drag and buoyancy.

$$\mathbf{F}_{total} = \mathbf{F}_G + \mathbf{F}_D + \mathbf{F}_B. \tag{4}$$

The drag force is determined, in order to satisfy the prescribed value of bubble slip velocity. The elastic coefficient for the collision between the bubble and the reactor wall is assumed to be 0.1.

Liquid dynamics: The following mass, momentum, and energy conservation equations are applied to the liquid phase, which is assumed to be an incompressible fluid.

$$\frac{\partial u_i}{\partial x_i} = 0 \tag{5}$$

$$\frac{\rho \partial u_i}{\partial t} + \frac{\rho \partial u_j u_i}{\partial x_j} = -\frac{\partial p}{\partial x_i} + \frac{\partial}{\partial x_j}\mu\frac{\partial u_i}{\partial x_j} - \rho g_i \beta\left(T - T_0\right) + \Phi \tag{6}$$

$$\frac{\rho C_p \partial T}{\partial t} + \frac{\rho C_p \partial u_j T}{\partial x_j} = \frac{\partial}{\partial x_j}K\frac{\partial T}{\partial x_j} + Q \tag{7}$$

where β is the thermal expansion coefficient of the liquid, T the liquid temperature, T_0 the temperature at the reactor bottom, F the momentum exchange between bubbles and liquid, and

K the heat transfer coefficient of the liquid. Q is the heat, which is generated by the reaction and is removed by the quench gas and the heat loss through the reactor wall. The effective viscosity, μ, is expressed as follows:

$$\mu = \mu_m + \mu_t \tag{8}$$

where μ_m is the molecular viscosity, and μ_t is the turbulent viscosity calculated by the following equation.

$$\mu_t = \tilde{C}_t \rho \frac{k^2}{\varepsilon}. \tag{9}$$

The heat transfer coefficient, K, in Equation (7) consists of the following two conductivities:

$$K = K_m + K_t \tag{10}$$

where K_m is the molecular thermal conductivity, and K_t is the turbulent thermal conductivity. The latter is estimated by

$$K_t = \frac{\mu_t C_p}{Prt} \tag{11}$$

where Prt is the Prandtl Number for turbulence and is taken to be 0.9 experimentally determined[27)]. In the MP k-ε model, the turbulence energy, k, and its rate of viscous dissipation, ε, are obtained by solving the following equations:

$$\frac{\partial \rho k}{\partial t} + \frac{\partial u_i \rho k}{\partial x_i} = \frac{\partial}{\partial x_i}\left(\frac{\mu_t}{\sigma_k}\frac{\partial k}{\partial x_i}\right) + G_s + G_T - \rho\varepsilon \tag{12}$$

$$\frac{\partial \rho\varepsilon}{\partial t} + \frac{\partial u_i \rho\varepsilon}{\partial x_i} = \frac{\partial}{\partial x_i}\left(\frac{\mu_t}{\sigma_\varepsilon}\frac{\partial \varepsilon}{\partial x_i}\right) + C_1\frac{\varepsilon}{k}\left(G_s + G_T\right)\left(1 + C_3 R_f\right) - C_2\frac{\rho\varepsilon^2}{k} \tag{13}$$

where $\sigma_k = 1.0$, $\sigma_\varepsilon = 1.3$, $C_1 = 1.44$, $C_2 = 1.92$, and $C_3 = 0.0$. Since C_3 is zero, the term of $C_3 R_f$ can be neglected. G_s, which characterizes MP k-ε model, is described as follows:

$$G_s = \rho \tilde{C}_t \frac{k^2}{\varepsilon} S\Omega \tag{14}$$

Where

$$S = \left\{ \frac{1}{2} \left(\frac{\partial u_i}{\partial x_j} + \frac{\partial u_j}{\partial x_i} \right) \left(\frac{\partial u_i}{\partial x_j} + \frac{\partial u_j}{\partial x_i} \right) \right\}^{\frac{1}{2}} \tag{15}$$

$$\Omega = \left\{ \frac{1}{2} \left(\frac{\partial u_i}{\partial x_j} - \frac{\partial u_j}{\partial x_i} \right) \left(\frac{\partial u_i}{\partial x_j} - \frac{\partial u_j}{\partial x_i} \right) \right\}^{\frac{1}{2}} \tag{16}$$

$$\underline{S} = \min\left(20, \frac{k}{\varepsilon} S \right) \tag{17}$$

$$\tilde{C}_t = \min\left(0.09, \frac{0.3}{1 + 0.35\underline{S}^{1.5}} \right) \tag{18}$$

$$G_t = g\beta \frac{u_t}{\sigma_t} \frac{\partial T}{\partial x_i} \tag{19}$$

$$R_f = \frac{-G_T}{G_s + G_T}. \tag{20}$$

$\underline{S}$ is the strain rate parameter summarized by Cotton and Ismael[28)].

The boundary conditions of Equations (12) and (13) are expressed by the following equations: The free-slip conditions are applied to the vertical planes including the central axis of the designated cell with an angle of 0.05 radian. The log-law conditions are applied to the boundary layers near the walls of the reactor based on Equations (1) and (2).

Free-slip condition;

at y = 0

$$\frac{\partial k}{\partial y} = 0 \tag{21}$$

$$\frac{\partial \varepsilon}{\partial y} = 0 \tag{22}$$

where y is the vertical distance from the boundary.

Log-law;

$$k = \frac{u^*}{\sqrt{C_t}} \tag{23}$$

$$\varepsilon = \frac{u^*}{\kappa y}. \qquad (24)$$

The dispersion of the tracer is expressed by the following diffusion equation:

$$\frac{\partial c}{\partial t} + \frac{\partial u_j c}{\partial x_j} = \frac{\partial}{\partial x_j} D_m \frac{\partial c}{\partial x_j}. \qquad (25)$$

The effective dispersion coefficient, D_m, consists of the following coefficients:

$$D_m = D_{mm} + D_{mt} \qquad (26)$$

where D_{mm} is the molecular dispersion coefficient, and D_{mt} is the turbulent dispersion coefficient. For the two-phase flow in the reactor, D_{mm} is much smaller than D_{mt} and can be neglected. D_{mt} can be estimated by

$$D_{mt} = \frac{\mu_t}{\rho\, Sct} \qquad (27)$$

where Sct is the Schmidt Number for turbulence and is assumed to be 0.9[29].

Momentum transfer: The momentum transfer rate from the bubbles to the liquid, Φ, is equal to the reciprocal of the drag force acting on the bubbles, F_D.

The above equations, which are described for a rectangular coordinate system, are transformed to a cylindrical coordinate system for purposes of this calculation.

4.3 Model Parameters

4.3.1 Operating Conditions

In the present study, the three operating conditions, cases 1, 2', and 4', in which the residence time distribution data were obtained by neutron absorption tracer technique, were analyzed.

4.3.2 Physical Properties of the Gas and Slurry

In the present study, the physical properties and the flow rates of the gas and slurry phases are shown in Table 4-1, because the operating conditions in cases 2' and 4' are slightly different from those in cases 2 and 4 shown in Section 2.2. Since there is no significant difference between the physical properties of the first and third reactors as shown in Table 4-1, the average properties were used in a reactor. The mean residence times of the slurry phase, determined by the tracer tests are shown in Table 2-8. The average flow rates of the slurry phase in the reactors were calculated based on the mean residence times and the gas holdups and, were used in the dynamic simulation, because these values were more accurate than the slurry flow rates estimated from the reaction simulator.

Table 4-1. Model parameters used for the calculations

	case 1	case 2'	case 4'
[the first reactor]			
density of gas, kg m^{-3}	20	48	45
density of slurry, kg m^{-3}	964	730	790
viscosity of gas, m Pa s	0.01	0.02	0.02
viscosity of slurry, m Pa s	7.0	0.7	0.7
heat capacity of slurry, J kg^{-1} K^{-1}	-	2680	2680
thermal conductivity of slurry, W m^{-1} K^{-1}	-	0.163	0.174
measured mean residence time, min.	29	30	39
gas holdup, -	0.56	0.56	0.56
flow rate of gas phase, m^3 h^{-1}			
at inlet	177	142	143
at outlet	177	182	185
average	177	162	164
flow rate of slurry phase, m^3 h^{-1}	8.65	8.41	6.59
averaged superficial gas velocity, m s^{-1}	0.063	0.057	0.058
averaged superficial slurry velocity,m s^{-1}	0.0031	0.0030	0.0023
[the third reactor]			
density of gas, kg m^{-3}		62	
density of slurry, kg m^{-3}		730	
viscosity of gas, m Pa s		0.02	
viscosity of slurry, m Pa s		0.4	
heat capacity of slurry, J kg^{-1} K^{-1}		2760	
thermal conductivity of slurry, W m^{-1} K^{-1}		0.140	
measured mean residence time, min.		27	
gas holdup		0.60	
flow rate of gas phase, m^3 h^{-1}			
at inlet		171	
at outlet		209	
average		190	
flow rate of slurry phase, m^3 h^{-1}		8.63	
superficial gas velocity, m s^{-1}		0.067	
superficial slurry velocity, m s^{-1}		0.0031	

4.3.3 Other Parameters

In order to perform the simulation, parameters and physical properties are estimated as follows:

(a) Under the liquefaction conditions of the EDS process [30)], the slip velocity was determined to be 0.09 m s^{-1} at superficial gas velocities lower than 0.07 m s^{-1}.

(b) The correlations of the gas holdup are shown in Section 2.4. In this study, based on the measured data, the gas holdup is assumed to be 0.56 in the first reactor and 0.60 in the third reactor where the gas velocity is high.

(c) The thermal expansion of the slurry phase is assumed to be 1.6×10^{-3} K^{-1} at 723 K. This value is estimated from Equations (1) and (2) of Section 2.3 and using the parameters shown in Table 2-4, for an oil fraction with a normal boiling point of 651 K.

(d) The heat generated in the reactor is determined so as to fit the temperature distributions measured in the first reactor, as shown in Table 2-2.

(e) The heat which is lost through the wall is estimated to be 1105 W m^{-2} based on the heat balance as shown in Section 3.3.5.

4.4 Solution Technique

The calculation was carried out for a cylindrical wedge of 0.05 radians, as shown in Figure 4-1. The number of elements was 20 for the radial direction and 180 for the axial direction, and the time step was 0.2 s. At the top and bottom parts, the grid sizes were reduced to deal with complex flows. The heat removal, which was caused by the gas injection to the reactor, was also considered in the calculation. All conservation equations were solved dynamically and numerically from the initial conditions;

(1) the temperature is equal to the feed temperature,
(2) the gas and liquid velocities are zero, and
(3) there are no bubbles.

To obtain steady state values, the calculation was continued for twice the mean residence time of the liquid for case 1 and triple that for cases 2' and 4'. Equation (25) was solved to obtain the tracer response curve at the outlet after a steady state flow was achieved. The tracer injection was expressed in the simulation as the concentration increase in the feed slurry for 15 s, with no affecting the hydrodynamics in the reactor.

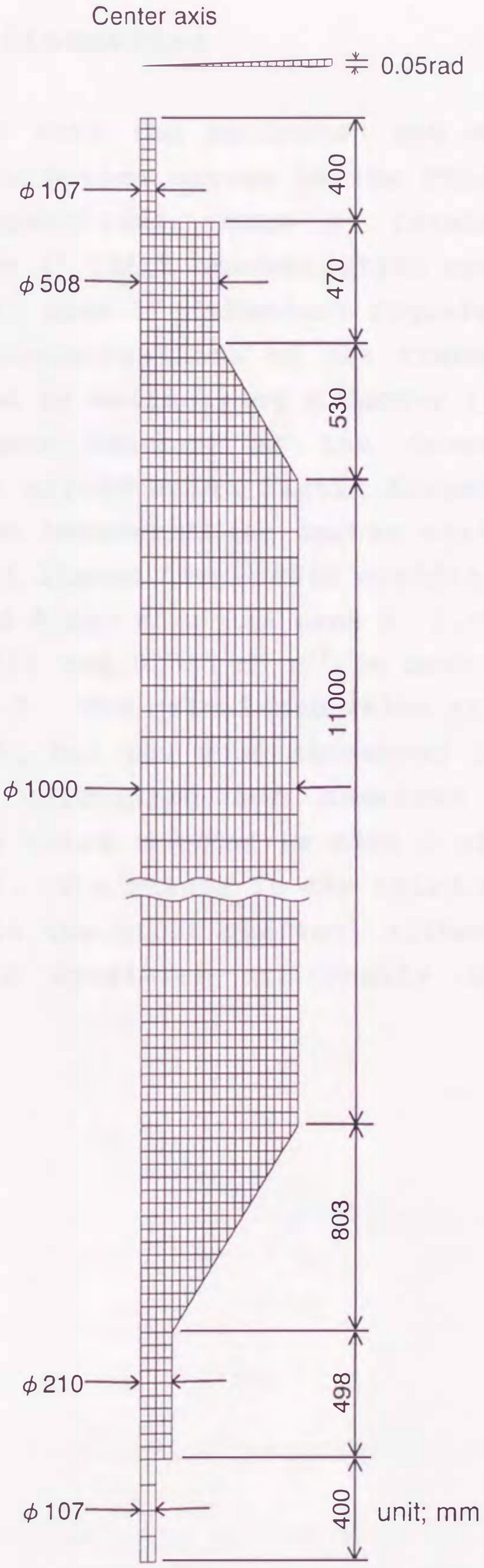

Figure 4-1. Sketches of the wedge and mesh used for calculation in the liquefaction reactor.

4.5 Results and Discussion

Figures 4-2 show the estimated and measured residence residence time distribution curves in the first reactor in case 1 (cold solvent operation), case 2' (standard liquefaction operation), and case 4' (high concentration operation-2), and in the third reactor in case 2' (standard liquefaction operation). The dimensionless concentrations of the tracer of the measured curves were adjusted by multiplying a factor (=1.0 to 1.2) so as to satisfy the mass balance of the tracer, because such adjustment does not affect axial liquid dispersion coefficients and makes comparison between these curves easier. The measured and calculated axial liquid dispersion coefficients in the first reactor are 0.11 and 0.067 m^2 s^{-1} in case 1, 0.029 and 0.028 m^2 s^{-1} in case 2', and 0.022 and 0.021 m^2 s^{-1} in case 4', respectively, as shown in Table 4-2. The calculated value is smaller than that measured for case 1, but the good agreement is found for cases 2' and 4'. The calculated and measured axial dispersion coefficients in the third reactor in case 2 are 0.039 and 0.050 m^2 s^{-1}, respectively. The values in the third reactor are 30-50% larger than those in the first reactor, although the flow rates and gas and liquid densities are nearly the same for both reactors.

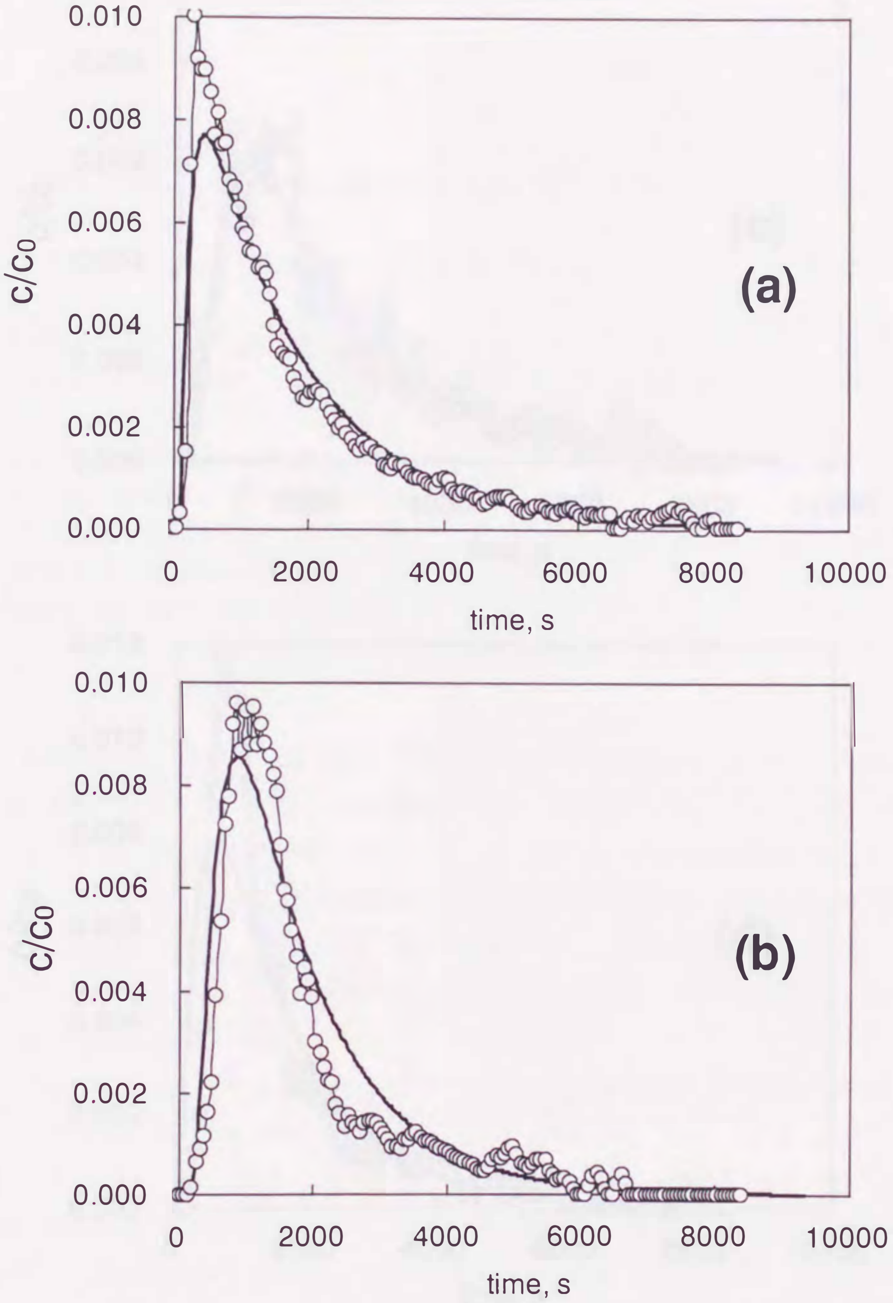

Figure 4-2. Residence time distribution in the reactors.
(a) in the first reactor for case 1,
(b) in the first reactor for case 2';
Thin lines, experimental; Solid lines, calculated.

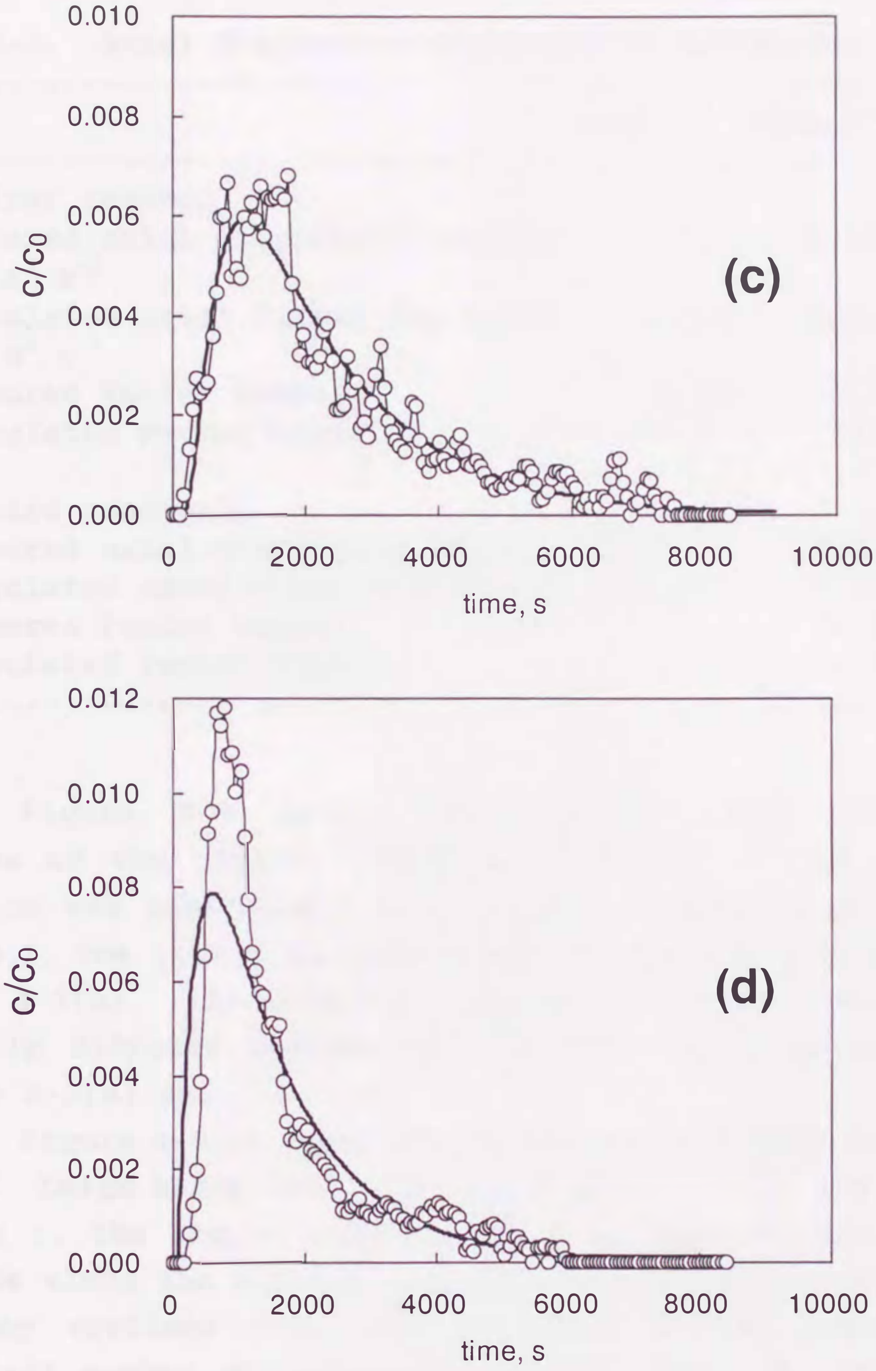

Figure 4-2. Residence time distribution in the reactors.
(c), in the first reactor for case 4'
(d), in the third reactor for case 2';
Thin lines, experimental; solid lines, calculated.

Table 4-2. Axial dispersion coefficients and Peclet Number

	case 1	case 2'	case 4'
[the first reactor]			
measured axial dispersion coeff., m^2 s^{-1}	0.11	0.029	0.022
calculated axial dispersion coeff., m^2 s^{-1}	0.067	0.028	0.021
measured Peclet Number	0.73	2.7	3.4
calculated Peclet Number	1.2	2.7	3.4
[the third reactor]			
measured axial dispersion coeff., m^2 s^{-1}		0.039	
calculated axial dispersion coeff., m^2 s^{-1}		0.050	
measured Peclet Number		2.2	
calculated Peclet Number		1.7	

Figure 4-3 shows the unsteady-state concentration patterns of the tracer, which was injected in the feed. The injection was continued for 15 s at a concentration of unity. In case 1, the tracer ascends along the central axis as shown in Figure 4-3(a). In cases 2' and 4', however, the tracer is gradually diffused during the ascending movement as shown in Figures 4-3(b) and (c).

Figure 4-4(a) shows the steady-state flow patterns of the liquid. Large black dots mean the points of cold gas injection. In case 1, the liquid ascends along the central axis and then descends along the annular region near the reactor wall. There are many vortices near the top cone of the reactor. The equivalent number of completely stirred tanks, N, calculated by Equation (15) of Section 2.5 is 1.4 by estimation and 1.3 by measurement. Both values are close to unity, indicating a strong circulation in the reactor. This circulation is probably initiated by the upward flow of the gas and slurry through the inlet nozzle at the bottom of the reactor.

In cases 2' and 4', however, the ascending flow in the central region is suppressed by strong, randomly occurring vortices as shown in Figures 4-4(b) and (c). The size of the vortices, shown in Figure 4-4, is in the range of 0.1-0.25 m. This range is in agreement with the vortex size, 0.17 m, determined by Tzeng et al.31) in a three-phase fluidized bed, operated for nitrogen-water systems at ambient conditions. The descending flow is found at the central area in cases 2' and 4'. The equivalent number of completely stirred tanks is 2.1 both by calculation and measurement in case 2', and 2.4 by calculation and 2.1 by measurement in case 4'. All these flow patterns show two or three circulation cells in the reactor. The difference on tracer spreading, shown in Figure 4-3, may be caused by the different flow patterns between case 1 and cases 2 and 3.

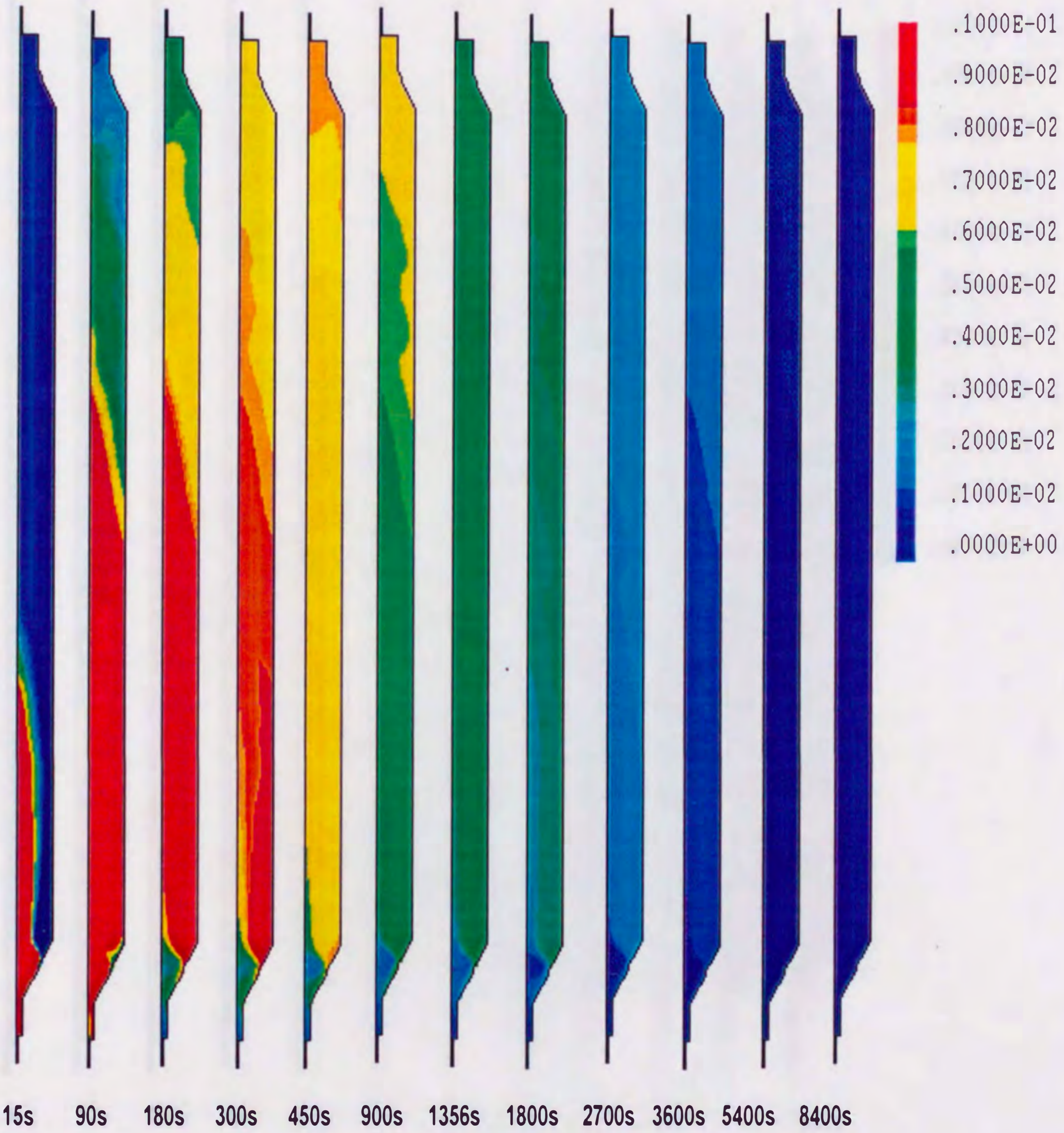

(a)

Figure 4-3 Estimated unsteady state concentration patterns of the tracer in the reactors.
(a), case 1 in the first reactor.

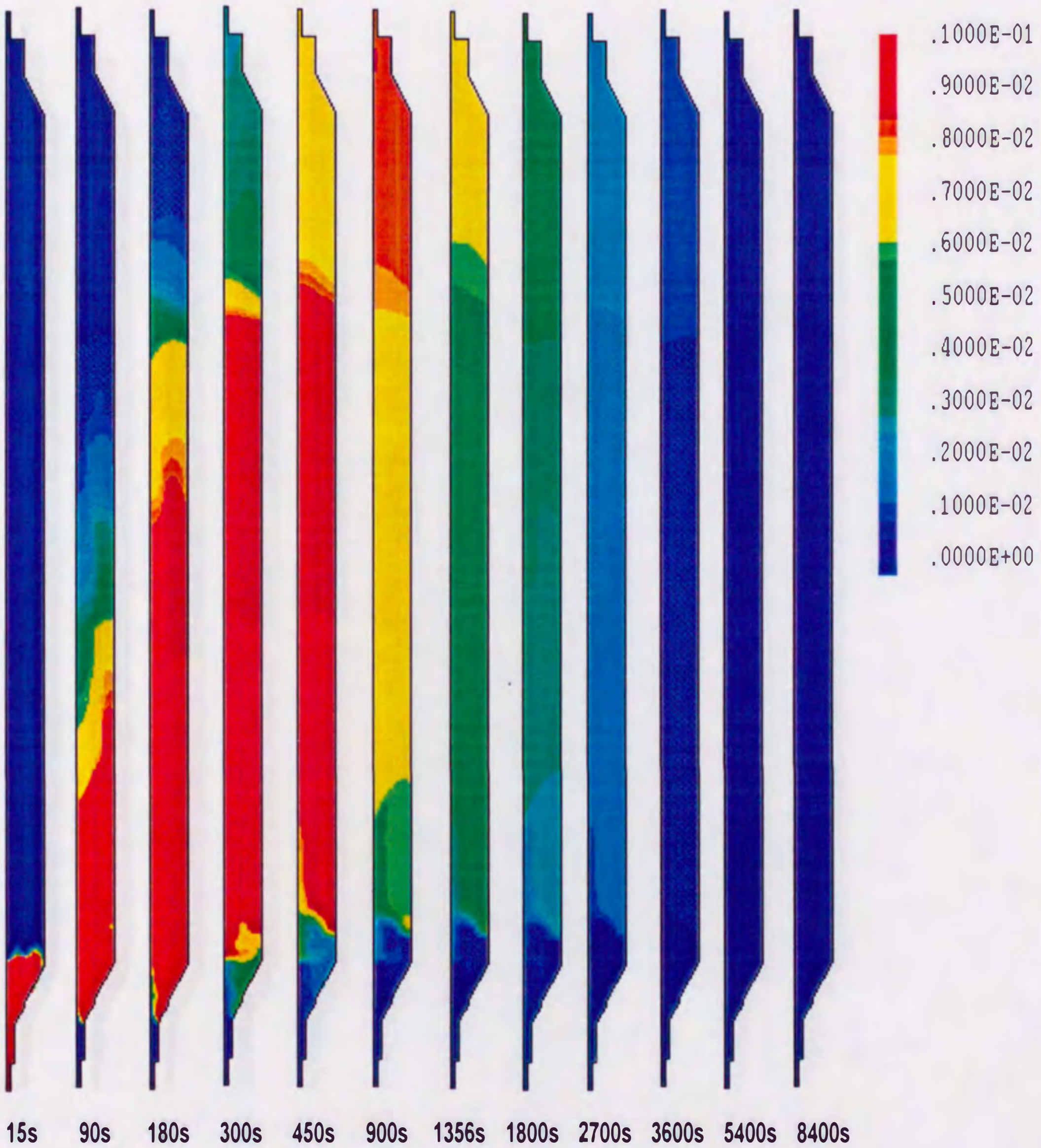

(b)

Figure 4-3 Estimated unsteady state concentration patterns of the tracer in the reactors.
(b), case 2′ in the first reactor.

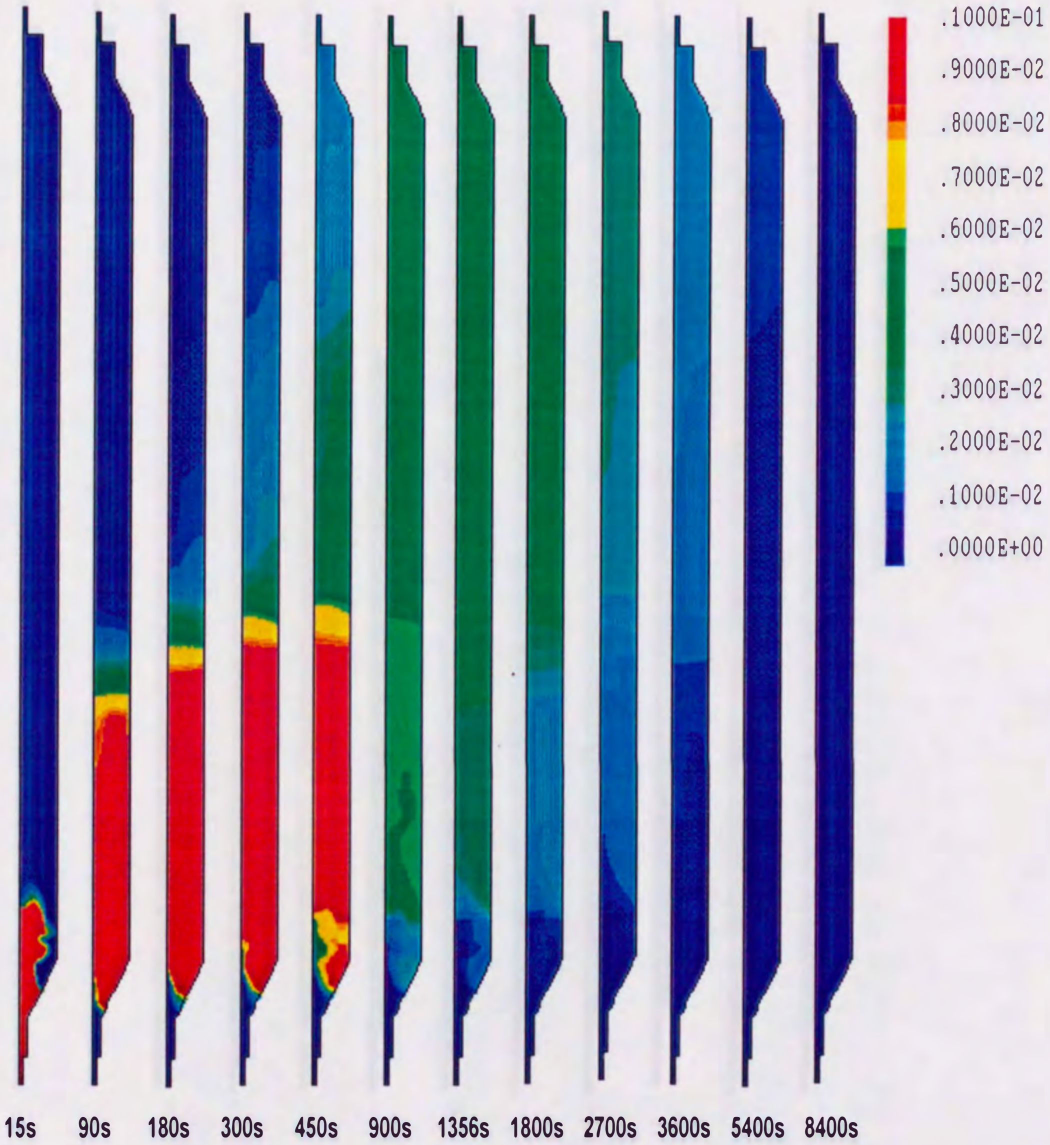

(c)

Figure 4-3 Estimated unsteady state concentration patterns of the tracer in the reactors.
(c), case 4′ in the first reactor.

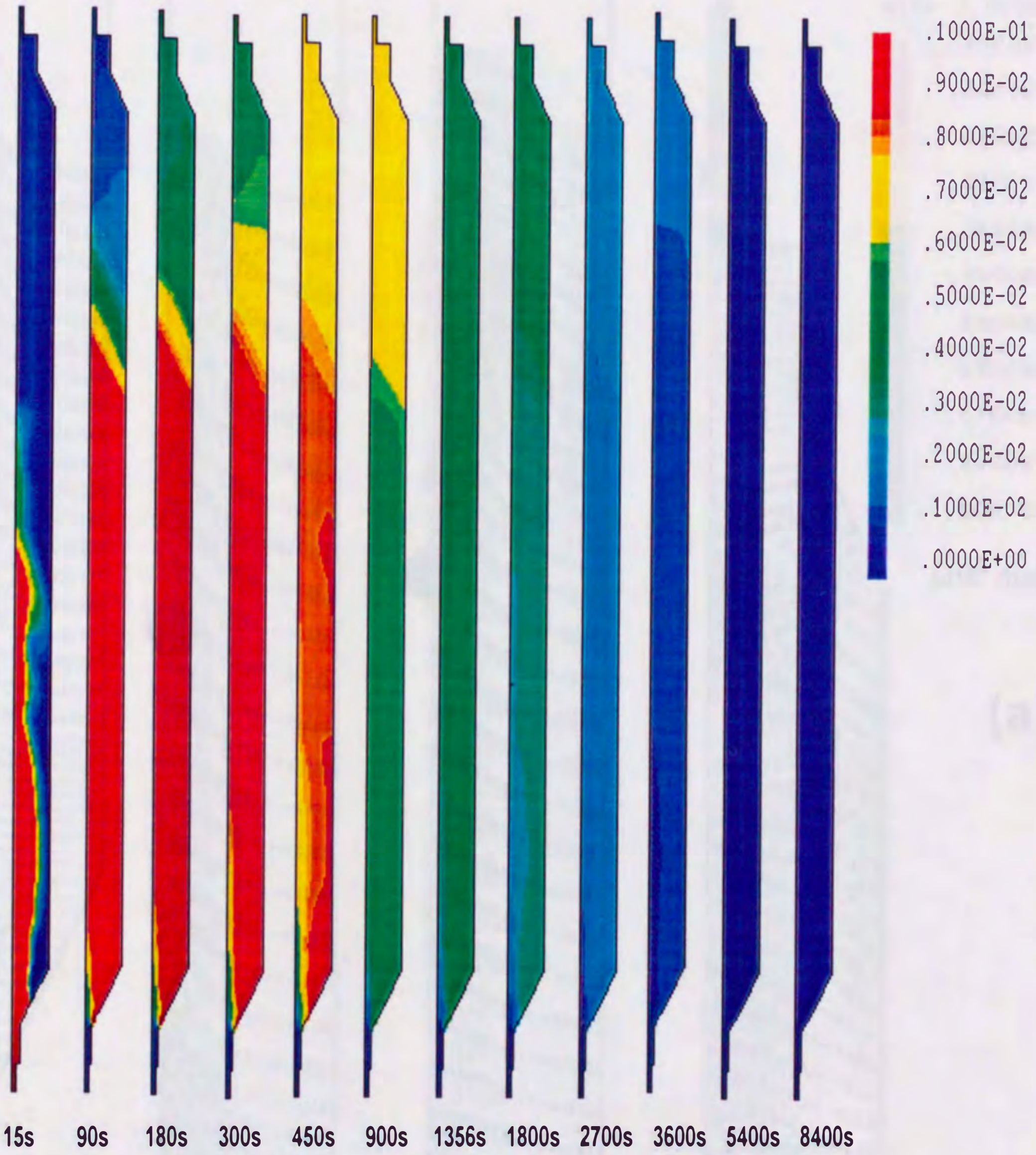

(d)

Figure 4-3 Estimated unsteady state concentration patterns of the tracer in the reactors.
(d), case 2′ in the third reactor.

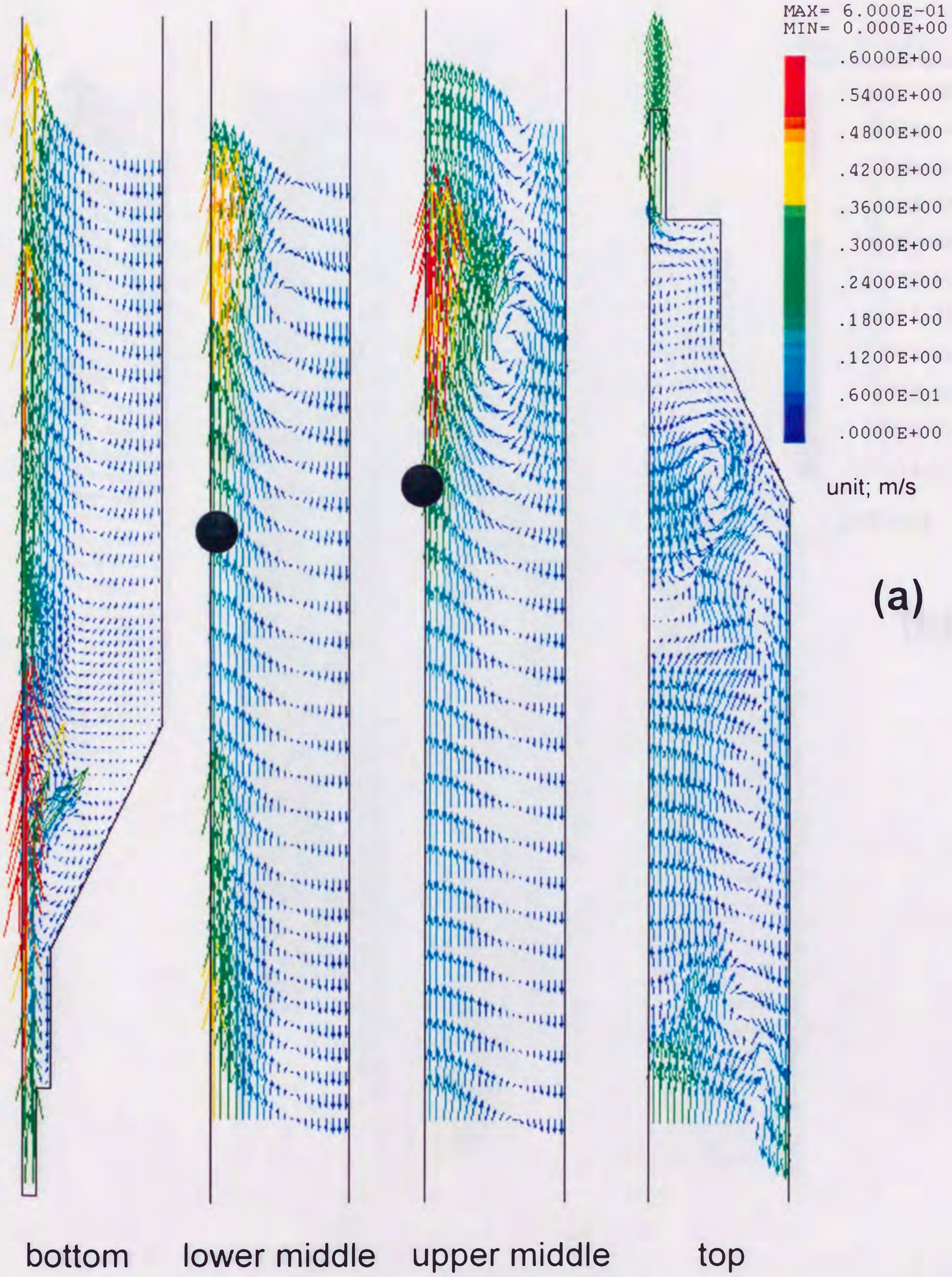

Figure 4-4. Estimated velocity patterns in the reactors. (a), case 1 in the first reactor.

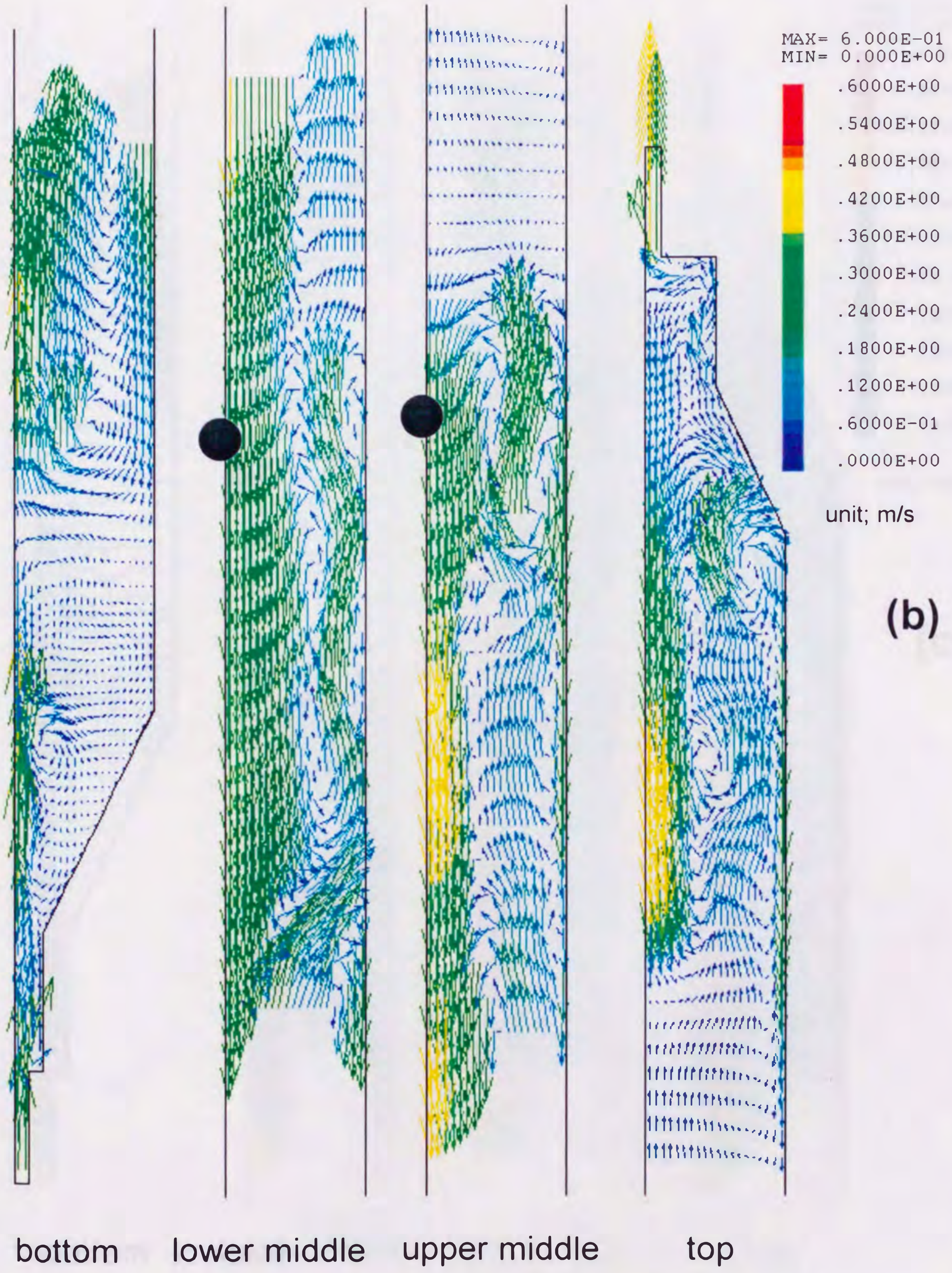

Figure 4-4. Estimated velocity patterns in the reactors.
(b), case 2′ in the first reactor.

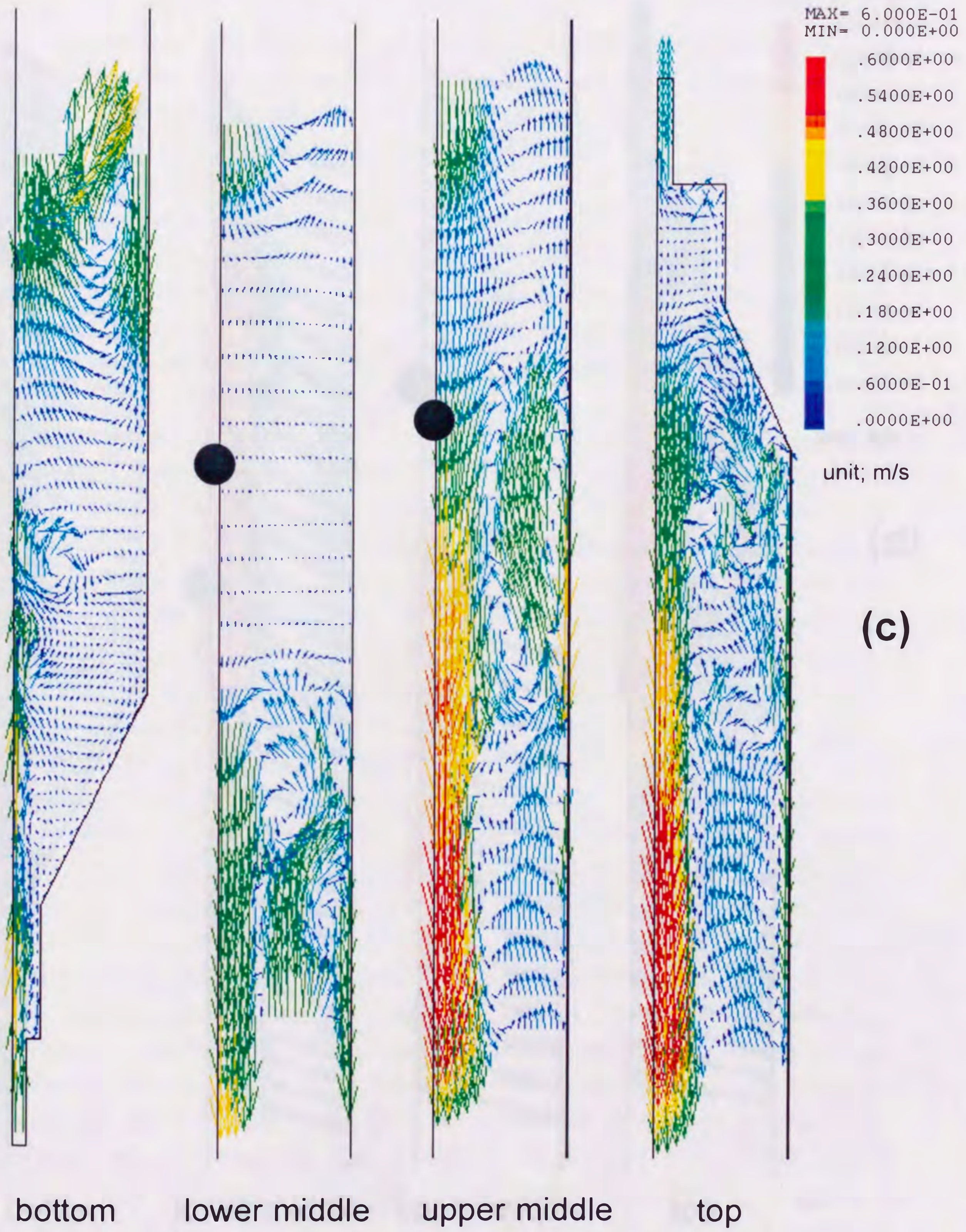

Figure 4-4. Estimated velocity patterns in the reactors. (c), case 4′ in the first reactor.

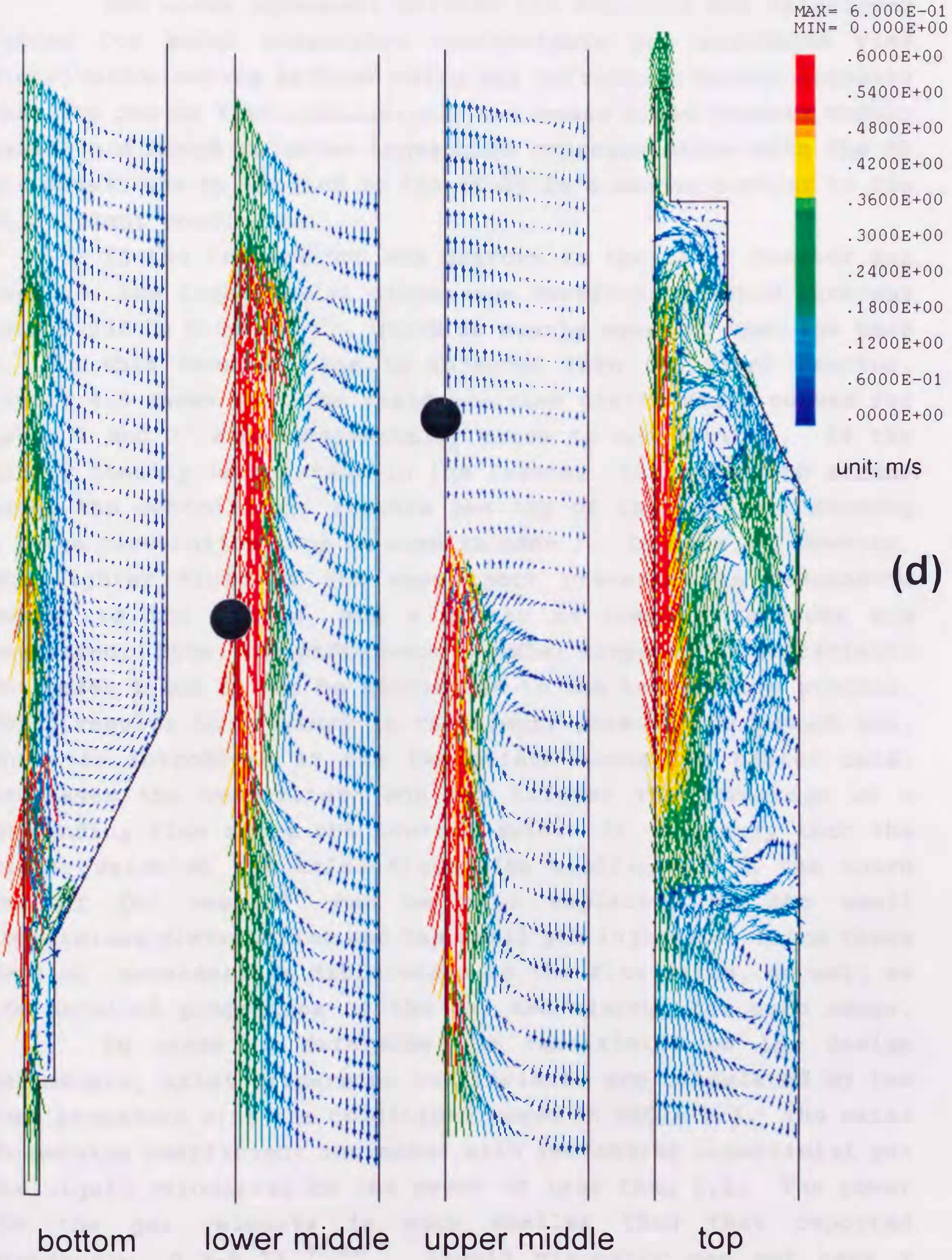

Figure 4-4. Estimated velocity patterns in the reactors.
(d), case 2′ in the third reactor.

The close agreement between the measured and calculated values for axial dispersion coefficients and residence time distribution curves without using any correction factor suggests that the pseudo-three-dimensional two-phase fluid dynamic model, based on a mixed Eulerian-Lagrangian representation with the MP k-ε model, can be applied to the study in a manner similar to the pilot plant conditions.

If the temperature was uniform in the first reactor for case 2', the liquid axial dispersion coefficient would increase from 0.032 to 0.051 $m^2\ s^{-1}$, which is nearly equal to that for case 1. In this case, no gas is injected into the first reactor. Figure 4-5 shows that the residence time distribution curves for cases 1 and 2' are fundamentally close to one another. If the slurry density is constant in the reactor, the ascending stream along the central axis reaches the top of the reactor, forming a large circulation loop as seen in case 1. In case 2', however, the lighter fluid at the upper part prevents the descending motion to the bottom, and a number of complex vortices are generated. Thus, the difference in axial dispersion coefficients for cases 1 and 2' can be attributed to the temperature profile, which results in buoyancy in the slurry phase. The quench gas, which is introduced at the two points along the center axis, decreases the temperature and may trigger the formation of a descending flow along the central axis. It is likely that the higher value of the axial dispersion coefficient in the third reactor for case 2' can be also explained by the small temperature distribution and the small gas injection, since there were no considerable differences in the flow rates, as well as the physical properties of the gas and slurry, for both cases.

In order to determine the sensitivity of the design parameters, axial dispersion coefficients are calculated by the same procedure with the conditions shown in Table 4-3. The axial dispersion coefficient increases with increasing superficial gas and liquid velocities to the power of less than 0.1. The power for the gas velocity is much smaller than that reported previously, 0.3-0.77 32,33). Liquid viscosity may not have a strong influence on the axial dispersion coefficient31). The diameter of the reactors also might not be predominant for reactors larger than 1 m. The axial dispersion coefficient for a 4-m diameter reactor is estimated to be only 40 % larger than that for a 1-m diameter reactor. The values measured at the Kashima pilot plant can, in practice, be applied to the design of a large-scale reactor (2-5 m in diameter).

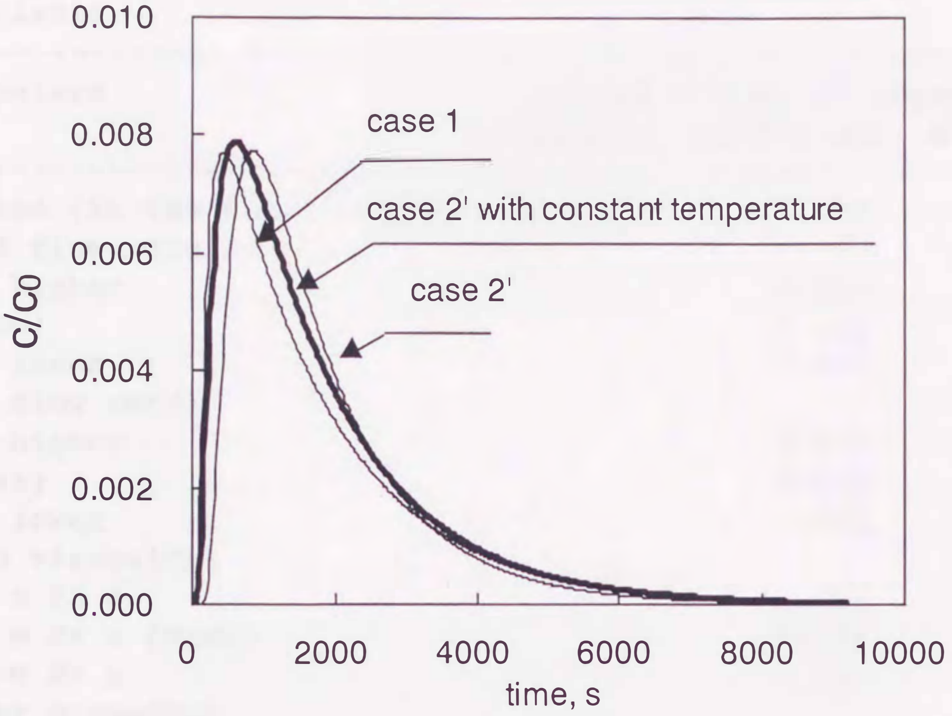

Figure 4-5. Calculated residence time distribution In the first reactor for case 1 and case 2'. Solid line, case 2' with constant temperature.

Table 4-3. Effect of design conditions on axial dispersion coefficients

Parameters	Calculated axial liquid dispersion coefficient, m^2 s^{-1}
base case (in the first reactor, case 2')	0.028
[liquid flow rate]	
20% higher	0.043
(base)	0.028
20% lower	0.020
[vapor flow rate]	
20% higher	0.036
(base)	0.028
20% lower	0.027
[liquid viscosity]	
7.0 m Pa s	0.016
0.7 m Ps s (base)	0.028
0.4 m Ps s	0.027
[reactor diameter]	
0.61 m	0.026
1.0 m (base)	0.028
2.0 m	0.024
4.0 m	0.039

4.6 Conclusions

A pseudo-three-dimensional two phase fluid dynamic model was developed based on a combined Eulerian-Lagrangian representation using the MP k-ε model for turbulence stresses and was applied to the liquefaction reactors at the Kashima pilot plant. The residence time distribution curves determined by the tracer injection were closely in agreement with those predicted by the dynamic simulation using a finite-volume solution algorithm. This suggests that the model is capable of providing the engineering description of the backmixing of the slurry under the coal liquefaction conditions at a superficial gas velocity of 0.06 m s^{-1} at 17 MPa. The simulation results also suggest that the axial dispersion coefficient is not greatly increased even if the diameter of the liquefaction reactor as increases four times that of the pilot plant reactor. The predicted flow patterns show that the temperature difference between the top and bottom of the reactor, as well as the introduction of the cold quench gas, was effective to decrease the axial dispersion coefficient of the liquid.

Nomenclature

A = constant, -
c = concentration of tracer, dimensionaless
Cp = heat capacity, J kg^{-1} K^{-1}
D_m = dispersion coefficient, m^2 s^{-1}
F_B = buoyant force acting on a bubble (vector), N
F_D = drag force acting on a bubble (vector), N
F_G = force acting on a bubble due to gravity (vector), N
F_{total} = total force acting on a bubble, N
g = gravitational constant, m s^{-2}
K = heat transfer coefficient, W m^{-2} K^{-1}
K_m = thermal conductivity, W m^{-1} K^{-1}
k = turbulent kinetic energy per unit mass, m^2 s^{-2}
m = parameter, -
N = equivalent number of completely stirred tanks, -
P_c = critical pressure, MPa
Pe = Peclet Number, dimensionless
Prt = Prandtl Number, dimensionless
Q = generated heat minus removed heat, J m^{-3} s^{-1}
R = gas constant, m^3 MPa kg-mol^{-1} K^{-1}
Sct = Schmidt Number, dimensionless
T = temperature, K
T_c = critical temperature, K
T_0 = base temperature, K
T_r = reduced temperature, dimensionless
t = time, s
u = velocity, m s^{-1}
u_i = velocity on i coordinate, m s^{-1}
u^* = friction velocity, m s^{-1}
u_b = bubble velocity (vector), m s^{-1}
u_l = liquid velocity (vector), m s^{-1}
u_{slip} = bubble slip velocity (vector), m s^{-1}
x_i = position on i-coordinate, m
Y = vertical distance from boundary, m
β = rate of thermal expansion of liquid, K^{-1}

ε = turbulent energy dissipation rate per unit mass, $m^2\ s^{-3}$
ε_g = gas holdup, -
κ = Karman constant, -
μ = viscosity, Pa s
ν = kinematic viscosity, $m^2\ s^{-1}$
ρ = density, kg m^{-3}
τ = mean residence time, s
τ_0 = shear stress, Pa

Subscripts
b = bubble
g = gas phase
i = i-coordinate
j = j-coordinate
l = liquid phase
m = molecular
s = solid
sl = slurry phase
t = turbulent

References

(1) Freedman, W.; Davidson, J.F. Hold-up and liquid circulation in bubble columns. *Transactions of the Institute of Chemical Engineers* **1969**, *47*, T 251.

(2) Joshi, J.B. ;Sharma, M.M. Some design features of radial baffles in sectionalized bubble columns. *The Canadian Journal of Chemical Engineering* **1979**, *57*, 375-377.

(3) Degaleesan, S.; Dudukovic, M.P.; Toseland, B.A.; Bhatt, B.L. A two-compartment convective-diffusion model for slurry bubble column reactors. *Ind. Eng. Chem. Res.* **1997**, *36*, 4670-4680.

(4) Degaleesan, S.; Dudukovic, M.P. Liquid backmixing in bubble column and the axial dispersion coefficient. *AIChE Journal* **1998**, *44*, 2369-2378.

(5) Schwarz, M.P.; Turner, W.J. Applicability of the standard k-e model to gas-stirred baths. *Applied Mathematics Modeling* **1988**, *12*, 273-279.

(6) Rizk, M.A.; Elgobashi, S.E. A two-equation model for dispersed dilute confined two-phase flows. *Int J. Multiphase Flow* **1989**, *15*, 119-133.

(7) Torvik, R.; Svendsen, H.F. Modelling of slurry reactors: A fundamental approach. *Chemical Engineering Science* **1990**, *45*, 2325-2332.

(8) Svendsen, H.F.; Jakobsen, H. A.; Torvik, R. Local flow structures in internal loop and bubble column reactors. *Chemical Engineering Science* **1992**, *47*, 3297-3304.

(9) Pan, Y.; Dudukovic, M.P.; Chang, M. Dynamic simulation of bubbly flow in bubble columns. *Chemical Engineering Science* **1999**, *54*, 2481-2489.

(10) Sanyal, J.; Vásquez, S.; Roy, S.; Dudukovic, M.P. Numerical simulation of gas-liquid dynamics in cylindrical bubble column reactors. *Chemical Engineering Science* **1999**, *54*, 5071-5083.

(11) Ranade, V.V. Flow in bubble column: some numerical experiments. *Chemical Engineering Science* **1992**, *47*, 1857-1869.

(12) Lapin, A.; Lübbert, A. Numerical simulation of the dynamics of two phase gas-liquid flows in bubble column. *Chemical Engineering Science* **1994**, *49*, 3661-3674.

(13) Devanathan, N.; Dudukovic, M.; Lapin, P.A.; Lübbert, A. Chaotic flow in bubble column reactors. *Chemical Engineering Science* **1995**, *50*, 2661-2667.

(14) Delnoij, E.; Lammers, F.A.; Kuipers, J.A.M.; van Swaaij,

W.P.M. Dynamic simulation of dispersed gas-liquid two-phase flow using a discrete bubble model. *Chemical Engineering Science* **1997,** *52*, 1429-1458.

(15) Delnoij, E.; Kuipers, J.A.M.; van Swaaij W.P.M. Dynamic simulation of gas-liquid two-phase flow: effect of column aspect ratio on the flow structure. *Chemical Engineering Science* **1997,** *52*, 3759-3772.

(16) Delnoij, E.; Kuipers, J.A.M.; van Swaaij W.P.M. A three-dimensional CFD model for gas-liquid bubble columns. *Chemical Engineering Science* **1999,** *54*, 2217-2226.

(17) Lain, S.; Bröder, D.; Sommerfeld, M. Experimental and numerical studies of the hydrodynamics in a bubble column. *Chemical Engineering Science* **1999,** *54*, 4913-4920.

(18) Majumdar, D.M.; Farouk, B.; Shah, Y.T. Hydrodynamic modeling of three-phase flows through a vertical column. *Chemical Engineering Science* **1997,** *52*, 4485-4497.

(19) Majumdar, D.M.; Farouk, B.; Shah, Y.T.; Macken, N.; Oh, Y.K. Two- and three phase flows in bubble columns: numerical predictions and measurements. *Ind. Eng. Chem. Res.* **1998,** *37*, 2284-2292.

(20) Krishna, R.; Urseanu, M.I.; van Baten, J.M.; Ellenberger, J. Influence of scale on the hydrodynamics of bubble columns operating in the churn-turbulent regime: experiments vs. Eulerian simulations. *Chemical Engineering Science* **1999,** *54*, 4903-4911.

(21) Onozaki, M.; Namiki, Y.; Sakai, Y.; Kobayashi, M.; Nakayama, Y.; Yamada, T.; Morooka, S. Dynamic simulation of gas-liquid dispersion behavior in coal liquefaction reactors. *Chemical Engineering Science* **1999,** submitted.

(22) Kato, M.; Launder, B.E. The modelling of turbulent flow around stationary and vibrating square cylinders. *Ninth Symposium on Turbulent Shear Flows* **1993,** No. 10-4.

(23) Luo, X.; Zhang, J.; Tsuchiya, K.; Fan, L.S. On the rise velocity of bubbles in liquid-solid suspensions at elevated pressure and temperature. *Chemical Engineering Science* **1997,** *52*, 3693-3699.

(24) Luo, X., Lee, D.J., Lau, R., Yang, G., & Fan, L.S. Maximum stable bubble size and gas holdup in high-pressure slurry bubble column. *AIChE Journal* **1999,** *45*, 665-680.

(25) Letzel, H.M.; Schouten, J.C.; Bleek, C. M. van den; Krishna, R. Influence of elevated pressure on the stability of bubbly flows. *Chemical Engineering Science* **1997,** *52*, 3733-3739.

(26) Schlichting, H. *Boundary-layer theory, 7th ed.*; McGraw-Hill:

New York, 1979.

(27) Versteeg, H.K.; Malalasekera, W. *An introduction to computational fluid dynamics*; Longman: England, 201, 1995.

(28) Cotton, M.A.; Ismael J.D. Development of a two-equation turbulence model with reference to a strain parameter. *Proc. 5th IAHR Conference on Refined-Flow Modelling and Measurement, Paris,* **1993.**

(29) Reynolds, A.J. The prediction of turbulent Prandtl and Schmidt Numbers. *Int. J. Heat Mass Transfer* **1975,** *18,* 1055-1069.

(30) Tarmy, B.L.; Chang, M.; Coulaloglou, C. A.; Ponzi, P. R. The Three Phase Hydrodynamics of the EDS Coal Liquefaction Reactors: Their Development and Use in Reactor Scaleup. *Inst. Chem. Eng., Sym. Ser.* **1984,** No.87, 303.

(31) Tzeng, J.W.; Chen, R.C.; Fan, L.S. Visualization of flow characteristics in a 2-D bubble column and three-phase fluidized bed. *AIChE Journal* **1993,** *39,* 733-744.

(32) Deckwer, W.D.; Burckhart, R.; Zoll, G. Mixing and mass transfer in tall bubble columns. *Chemical Engineering Science* **1974,** *29,* 2177-2188.

(33) Hikita, H.; Kikukawa, H. Liquid-phase mixing in bubble columns: effect of liquid properties. *The Chemical Engineering Journal* **1974,** *8,* 191-197.